ministerie van verkeer en waterstaat

koninklijk nederlands meteorologisch instituut

Turbulent exchange coefficients over a Douglas fir forest

F.C. Bosveld

Scientific reports; WR-91-02
Wetenschappelijke rapporten; WR-91-02

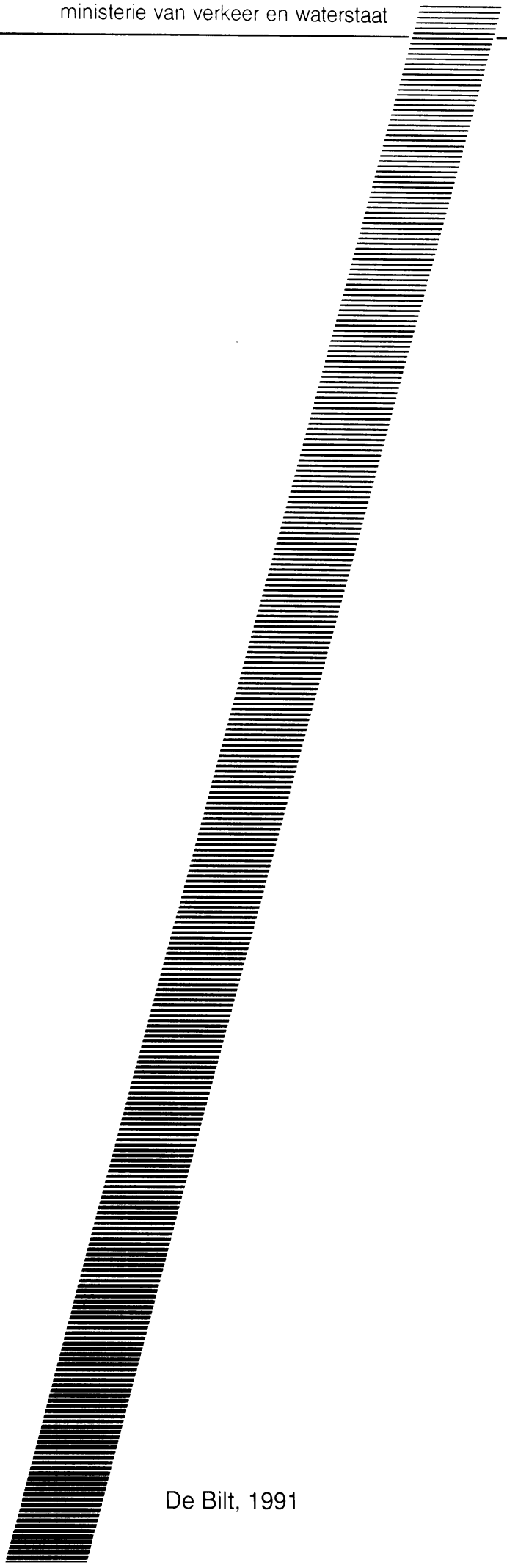

De Bilt, 1991

de bilt 1991

publicatienummer: Scientific reports=wetenschappelijke rapporten; WR-91-02 (FM)

postbus 201
3730 AE de bilt
wilhelminalaan 10
tel. (030) 206911
telex 47096
fax (030) 210407

Physical Meteorology Department

Turbulent exchange coefficients over a Douglas fir forest

auteur: F.C. Bosveld

U.D.C.: 551.551.8 551.577.13
551.584.41 630

ISSN: 0169-1651

ISBN: 90-369-2006-X

Turbulent exchange coefficients over a Douglas fir forest

F.C. Bosveld

Scientific reports; WR-91-02
Wetenschappelijke rapporten; WR-91-02

De Bilt, 1991

Contents

1. Introduction

Over the years flux-profile relations have been determined over various kinds of vegetation. Only a few studies are devoted to these relations over forest. The reason is clear. In general the complexity of forest sites give rise to advective influences for which especially profiles are very sensitive. As a consequence of fetch, profiles are measured at heights which are not or only partly exceeding the roughness layer above the forest. Due to advection effects local fluxes are only partly related to the local measured profiles, while roughness-layer effects give substantial deviation from the classical flux-profile relations over ideal terrain. Because a theoretical framework is missing any generalization of the experiments to other sites is difficult. For the determination of air pollutant fluxes to forest one often has to rely on profile measurements, since fast-response sensors necessary for the eddy-correlation technique are lacking. A determination of the site specific flux-profile relation is then unavoidable.

Within ACIFORN, a sub project of The Dutch Priority Program on Acidification, a project was formulated to determine the turbulent exchange coefficients over the Speulderbos location. This report gives a description of the experiments performed during 1989. Emphasis is on the formulation of the results in a form suitable for the derivation of fluxes of air-pollution components from profile measurements.

In chapter 2 an outline of surface layer similarity theory is given together with the main limitations for its use over a forest. Chapter 3 describes the instruments and their accuracy in relation to the desired accuracy for obtaining reliable flux-gradient relations. In chapter 4 the measurements are presented together with an analysis of the main factors that influence the turbulent exchange over the forest. In this chapter a simple extension of the usual flux-gradient relations is proposed to incorporate the main observed features. Chapter 5 gives a simple recipe for calculating fluxes from profile measurements. In chapter 6 auxiliary measurements made on a second mast in the forest are analysed to get an impression of the homogeneity of the flux and gradient fields over the forest stand. Chapter 7 summarise the main conclusions of this investigation. Two appendices are included. One on the influence of finite averaging time on the derived flux-gradient relations and one on the sensitivity of the results on the choise of the displacement height.

2 Theory

2.1 Similarity theory of the atmospheric surface layer

For horizontal homogeneous conditions it is assumed that in the atmospheric surface layer fluxes and vertical gradients are related to each other. To arrive at a relation between the turbulent flux F_c and the profile C(z) of a quantity C we write down the flux gradient relation:

$$F_c = - K_c \cdot \frac{\partial C}{\partial z} \tag{1}$$

where z is the height above the earth surface and K_c is the turbulent exchange coefficient. K_c can be written as the product of a turbulent velocity scale v_* and a turbulent length scale l:

$$K_c = v_* \cdot l \tag{2}$$

The velocity and length scale are related to the transporting turbulent eddies. We can argue that for
- horizontal homogeneous conditions
- $z >> h$ (the vegetation height)
- $z << z_i$ (the atmospheric boundary layer height)

the length scale of the transporting turbulent eddies is proportional to z (the height) itself. For the velocity scale the friction velocity u_* can be chosen. Indeed if we write:

$$K_c = k \cdot u_* \cdot z \tag{3}$$

and solve eq. 1 we arrive at the well known logarithmic profile for neutral conditions. In fact k (the Von Karman constant) is an empirical constant and chosen here to be 0.4.

For non-neutral conditions which are the more common conditions encountered, Monin and Obhukov introduced a second length scale L which is connected to the production (or destruction) of turbulent kinetic energy by buoyancy.

$$L = - \frac{\rho_a \cdot u_*^3}{k \cdot g \cdot \langle w' \rho_a' \rangle} \tag{4}$$

ρ_a density of air
g acceleration of gravity at the earth surface
$\langle w'\rho'_a \rangle$ turbulent air-density flux

The turbulent air-density flux is related to the temperature and humidity flux because both quantities act on the density of the air. For diabatic conditions we can form a new dimensionless parameter $\zeta = z/L$ and eq. 3 can be generalized to:

$$K_c = k \cdot u_* \cdot z \cdot \phi_c^{-1} (\zeta) \tag{5}$$

Where ϕ_c is the dimensionless gradient of the quantity C defined by :

$$\frac{k \cdot z}{c_*} \cdot \frac{\partial C}{\partial z} = \phi_c (\zeta) \tag{6}$$

The dimensionless functions ϕ for momentum and heat are experimentally determined over low vegetation by several authors. Here we use the well known Dyer and Hicks relations (Dyer, 1974) for the unstable case:

$$\phi_H(\zeta) = \phi_M^2(\zeta) = (1 - \gamma \cdot \zeta)^{-1/2} \tag{7}$$

where the subscripts H and M stand for heat and momentum respectively and $\gamma = 16$.

For the stable case it is generally found that $\phi_H = \phi_M$. However for the more stable situation ($\zeta > 0.5$) a deviation from the classical linear behaviour is found by Hicks (1976) and Carson and Richards (1978). Van Ulden and Holtslag (1985) expressed their findings in an analytical expression for the integrated flux-gradient relation. Here we use a functional form wich is very close to theirs but for which the parameters are more easy to interpret:

$$\phi_H(\zeta) = \phi_M(\zeta) = 1 + \beta\zeta_o \cdot (1 - e^{-\zeta/\zeta_o}) \tag{8}$$

where $\beta = 5.6$ and $\zeta_0 = 0.87$.

For gases it is assumed that the turbulent exchange process is the same as for heat, so:

$$\phi_H(\zeta) = \phi_c(\zeta) \tag{9}$$

for both stable and unstable situations.

2.2 The roughness layer

For the moment we will confine ourselves to neutral conditions and explore the limits of the applicability of eq. 3. What happens if we go down to the surface and violate the condition $z >> h$. As long as we stay above the top of the vegetation no flux is destroyed and it can be considered constant with height. Eq. 3 states that the length scale will decrease linearly while approaching the vegetation. However in the neighborhood of the vegetation turbulence is generated by the individual trees on a length scale c which relates to the wake generating parts of the trees. We expect the turbulent length scale to increase relative to its undisturbed value. This will result in a decrease of the dimensionless gradient.

Experimentally this effect has been found by Garret (1978), Raupach (1979), Denmead (1985), Högström et al. (1989) and Fazu and Schwerdtfeger (1989). However no clear picture arises of how to generalise the results.

2.3 Internal Boundary layers

Having discussed the deviation at the lowest part of the surface layer we now turn to the upper side. Often a forest is surrounded by less rougher terrain at a distance of some kilometers. The transition from a smooth to a rough terrain gives rise to an internal boundary layer in which the fluxes and profiles adapt to the new local terrain roughness.

To estimate the height of the equilibrium layer Businger (1986) gives as a rule of thumb for the fetch to height ratio 1:100, which means that with an upwind transition at 1 km distance the profiles and fluxes are in local equilibrium with the local terrain conditions up to a height of 10 m.

To be more quantitative we have to rely on numerical models for the inhomogeneous surface layer which allow for advection of the turbulent characteristics from the upwind terrain. The simplest models that can do the job properly are based on so-called E-ε closure,

sometimes called 1.5 order closure. Here we used such a model as described in Beljaars et.al. (1987) and Bosveld and Beljaars (1987).

We applied the model to estimate the effects on the exchange coefficient if a transition from smooth terrain to forest is present in the upwind terrain. The following assumptions are made :
- stability is neutral
- the exchange coefficients are equal for momentum, heat and trace gases.

The transition is chosen at 1.5 km upwind and is characterized by a roughness change from 0.15 to 1.5 m. The upwind terrain friction velocity was chosen as 0.5 m/s. In fact this is the situation at the Speulderbos location for the east sector.

Figure 1 shows the dimensionless shear. At 30 m height i.e 18 m above the displacement height (see section 4.2), this quantity deviates about 20% from the undisturbed value. This means that for profile derived flux estimates we would overestimate the friction velocity with 20%.

This analysis shows in a qualitative way that we are often in a position that the region where the usual flat terrain relations hold has schrunk to zero.

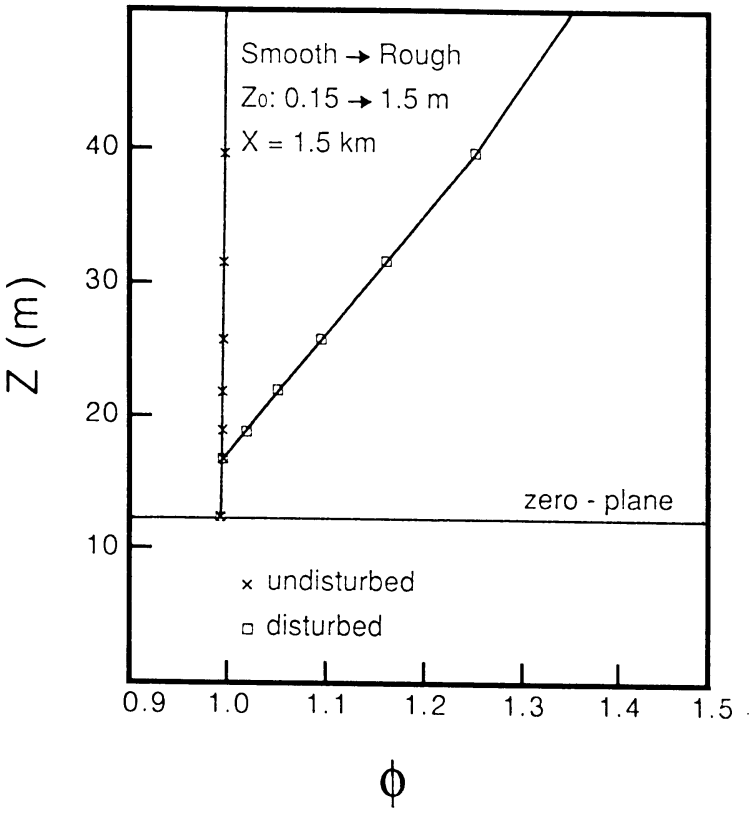

Figure 1.
Model calculation of the dimensionless shear for a smooth to rough transition (z_o from 0.15 to 1.5m) 1.5 km upstream.

3. Experimental setup

3.1 General considerations

The measurements of profiles over forest constitute a big experimental problem. Since the turbulent intensity is relatively high over such a rough terrain the profiles are very flat. This is even further enhanced by the presence of the roughness layer. For this reason even more than normal care is needed with respect to calibration and operational practice.

To get some appreciation of the desired accuracy in the temperature profile, the observed potential temperature difference between z = 31 and 24 m is plotted in figure 2 as a function of the sensible heat flux (H). For daytime situations the difference seldom exceeds 0.15 Kelvin. To estimate dimensionless gradients with an accuracy better than 10% the temperature differences should have an accuracy of circa 0.01 Kelvin.

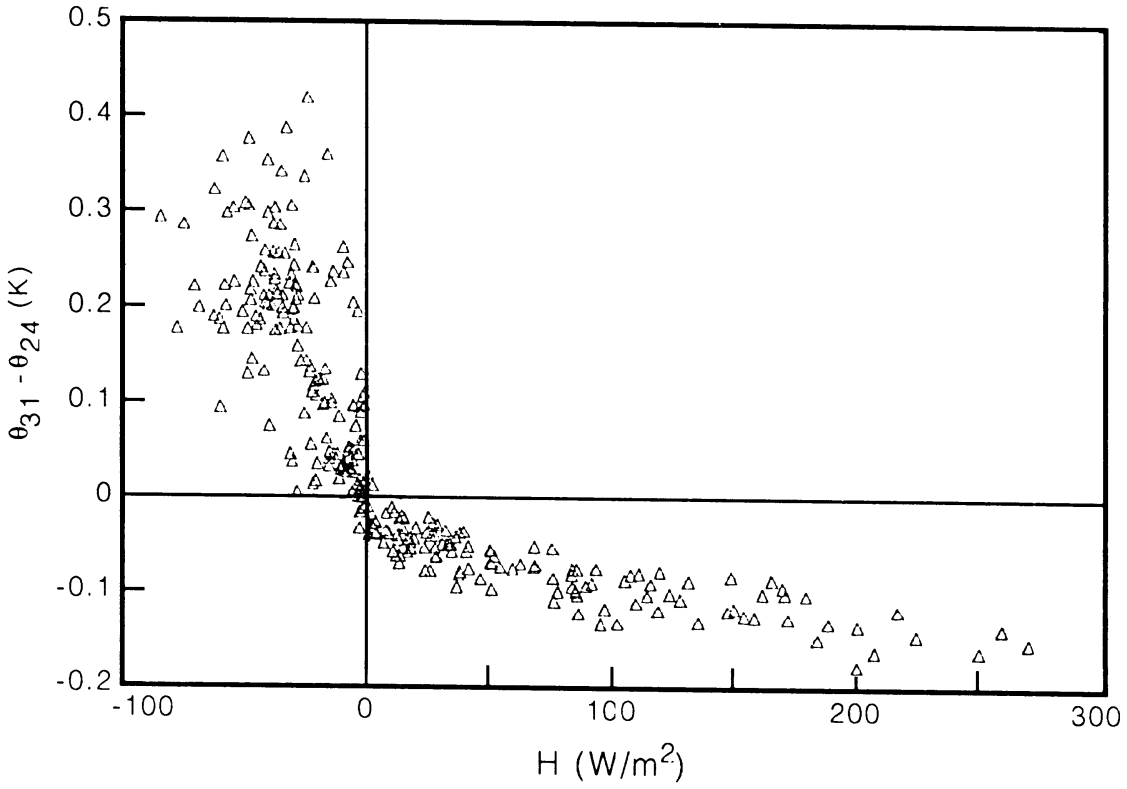

Figure 2.
Potential temperature (θ) difference between z=31 and 24 m as function of heatflux (H).

3.2 The mast

A 36 m mast is guyed on three sides at three levels. It has a triangular basis with sides of 1.2 m and consists of 6 identical segments. On each measuring level (36, 31, 24, 18 and 4 m for the profile and 30 m for the turbulence measurements) there is a working platform inside the mast. Cup-anemometers and turbulence sensors are mounted 3 m from the center of the mast and thermometers at 2.5 m. The effective diameter of the mast for potential flow is circa 0.3 m.

Table 1 give the exact measuring heights above the forest floor. In table 2 the instruments on the tower are listed. In the subsequent paragraphs the instruments used in the analysis of the flux-profile relations are described in more detail.

Level	Temp.	Wind
4	35.49	35.94
3	30.51	30.96
2	23.67	24.12
1	17.67	18.12

Table 1. Measuring heights (m) above forest floor of the profile instruments.

3.3 Instruments

Cup Anemometers

Wind speeds for the profile are measured with three conical cup anemometers fabricated at the Agricultural University of Wageningen (the Netherlands). The response length is circa 2 m/s and the threshold speed circa 0.3 m/s.

From the successive calibrations it was found that no significant change of the sensitivity occured during the experiments. The threshold speed however did increase slightly. The calibrations did show a slightly non-linear sensitivity. Because wind speeds seldom exceeds 11 m/s at the Speulderbos location it was decided to use a linear regression based on the calibration interval 0 - 11 m/s.

Inspection of the regression coefficients and the individual calibration data indicate that the error in the wind differences is less then 5 cm/s. For wind speeds lower then 1 m/s the linear calibration curve is not reliable. These data are excluded from the analysis. Stalling of the cup-anemometers was not detected since only 10 minute averages and standard deviations of the wind speeds were retained for analysis. The criterion of windspeed > 1 m/s is thought to be severe enough to exclude periods with stalling. No correction has been made for overspeeding.

Instrument	Type	Level (m)
Fast response		
1 Sonic anemometer	Kayo Denky	30
1 Pt-wire thermometer	KNMI	30
1 Ly-a hygrometer	ERC	30
Slow response		
5 Cup anemometers	LUW	36, 31, 24, 18, 4
5 Cu/Co thermo-couples (dry bulb)	KNMI	36, 31, 24, 18, 4
5 Cu/Co thermo-couples (wet bulb)	KNMI	36, 31, 24, 18, 4
2 Pt500 thermometers (abs. ref)	KNMI	18, 4
1 Wind vane	KNMI	36
1 Global radiation	Kipp	36
1 Net radiation	Funk	36
1 Infrared thermometer	Heimann	36
1 Scintillometer	KNMI	36
1 Rain detector	KNMI	36

Table 2.Instrumental equipment on the KNMI tower at the Speulderbos location.

Sonic Anemometer

Wind speed and temperature fluctuations are measured with a Kayo Denky sonic anemometer DAT 310. The probe was mounted on a thin 1 m high stem to diminish flow obstruction. The sonic probe is calibrated every two years. No significant deviations were found in successive calibrations.

u_* values are corrected for flow obstruction around the probe as derived in Duyzer and Bosveld (1987). Further a correction was applied for the angle dependency of the in horizontal wind speed sensitivity.

Sonic temperature fluctuations are corrected for moisture and horizontal wind speed influences as described by Schotanus et al. (1983).

Wind direction

Wind direction is measured with a standard KNMI vane. The angle calibration curve of the instruments showed a deviation of maximal 0.4 degree. The geographical direction of the zero-point of the instruments was measured with an accuracy of 1.5 degrees. No correction was applied.

Temperature

Dry- and wet-bulb temperature differences are measured with Copper-Constantane thermo-couples, while 4-wire Pt500 elements provide the thermo-couple reference to the absolute temperature. The Pt500 elements are thermally connected to the thermo-couples in an Aluminium block. The thermo-couple chain above the forest is closed. This means that we can check the system by adding all temperature differences in the chain. By proper operation this should sum up to zero.

The thermo-couples and its shielding is a modified version of the Cabauw type sensors as described by Slob (1978). The cotton sleeves of the wet-bulb sensors are continuously wetted with demineralised water by means of a small pump. All thermo-couple junctions were made of from one sample of copper and constantane wire. Calibration showed that there was no significant difference between the individual junctions. Consequently the same calibration curve could be used for all the elements.

Accuracy for the dry-bulb temperature differences is estimated at 0.02 Kelvin under normal conditions. The accuracy in the wet-bulb temperature is not clear at this time. The absolute temperature has an accuracy of 0.2 K.

4. Results

4.1 Introduction

Since we are dealing with micro-meteorological measurements close to the vegetation and in non-uniform terrain we may expect that classical surface layer similarity theory will not hold. Here we are interested in the deviations from similarity theory. The way to proceed is to present the data in the usual scaled way and discuss the observed discrepanties. To compare the results we generalize the equations 7 and 8 for ϕ to:

$$\zeta < 0 \qquad \hat{\phi}_{H,M} = \alpha \cdot \phi_{H,M}$$

$$\zeta > 0 \qquad \hat{\phi}_{H,M} = \alpha + (\phi_{H,M} - 1) \tag{10}$$

where α can be adapted to deviations caused by roughness layer effects.

Data selection criteria

For the determination of the dimensionless gradients of wind and temperature, half hour mean values were selected from the period April 1989 to January 1990. Selection on the data was performed to guarantee good instrumental performance. The criteria are:

for ϕ_M

1) no rain
2) U(z=18m) > 1 m/s
3) |DD-φ(sonic)| < 60°

where DD is the average wind direction and φ(sonic) the direction of the principle axis of the sonic. Criterium 3 is because the azimuth correction can only be applied to a limited angle of attack.

Some extra criteria for ϕ_H

4) potential temperature profile definite de- or increasing
5) $|\Delta\theta_{43}| > 0.05$ K
6) $|\langle w\theta \rangle| > 0.015$ Km/s

The last three criteria also exclude periods with rapid changing thermal conditions, especially during sunrise and sunset. Obstruction regarding the profiles due to mast interference at all levels in the profile occurs for wind direction between -30° and +30°. The lowest level (z = 18 m) of the profile measurements is obstructed for wind direction from 150° to 240°, due to a nearby tall tree. These wind sectors are excluded from the analysis.

4.2 Displacement height

The height above the vegetation serves as a scaling parameter for the turbulent characteristics. Therefore we must define a reference- or displacement height (d). Above the roughness layer the displacement height can be determined from the logarithmic profile for momentum. Since we have no profile measurements well above the roughness layer, the displacement height has to be determined in a different way. As a rule of thumb d is often

estimated as 2/3·h, h being the vegetation height. However this factor is found to be a function of vegetation density. The more dense the vegetation the higher this factor. Thom (1971) has experimentally identified the zero-plane with the level of action of drag on the vegetation. This was done however for a very simple artificial vegetation. Jackson (1981) has tried to give Thoms findings a more theoretical basis. Here we shall use the rule of thumb, which means for the KNMI-mast d = 12.5 m, tree height being circa 18 m.

4.3 Aerodynamic roughness length

The roughness length z_0 arises in the description of the wind velocity profile. Over homogeneous terrain, during stationary and neutral conditions and if remote enough from the individual roughness elements the wind profile can be described with the well known logarithmic formula:

$$U(z) = \frac{u_*}{k} \cdot \ln\left(\frac{z-d}{z_0}\right) \qquad (11)$$

where:
u. friction velocity
k von Karman constant
z height above earth surface
d zero-plane displacement
z_0 roughness length.

The roughness length is a measure for the power of the surface to destruct momentum. Its value for a particular terrain is used to estimate the friction velocity from a wind observation and an estimate of the atmospheric stability (Holtslag and van Ulden 1982).

An inspection of the Speulderbos site makes it likely that the roughness length is wind direction dependent. If we assume that the highest level of the profile measurements (z = 36 m) is above the roughness layer, an issue which will be discussed after the presentation of the dimensionless shear, then z_0 can be determined from the measurements by classification of the measurements into wind direction sectors of 30° and the ratio of U and u. around neutral.

Figure 3 shows the results. Very high values are found for the west sector ,which corresponds with the on eye observation from the mast. The other sectors give lower values although still higher then z_0 = 1 m, a value that is often quoted for forests.

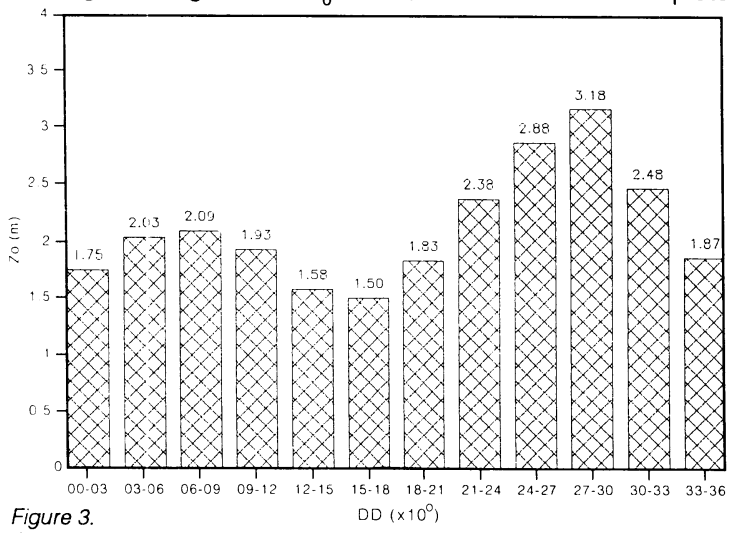

Figure 3.
Aerodynamic roughness length (z_0) as a function of wind direction class (DD).

4.4 Dimensionless gradients

Calculating the dimensionless gradients

For the calculation of the gradient from differences in the profile of a quantity M, which in our case stand for U or θ, between $z = z_2$ and $z = z_1$ we use the logarithmic approximation as outlined by Arya (1991):

$$\frac{dM}{d\ \ln(z-d)}\left(z = z_{eff} = \sqrt{(z_1-d)\ (z_2-d)}\right) \cong \frac{M_2 - M_1}{\ln (z_2-d) - \ln (z_1-d)} \qquad (12)$$

where z_{eff} is the effective height of the height interval. He shows that for the ratio of measuring heights above displacement height $(z_2-d) / (z_1-d) = 2$, the systematic error is < 2% for the stable case and < 0.4% for the unstable case. A ratio of two between successive profile levels occur in our case at the lowest levels of the profile. For higher levels in our profile the errors are even smaller.

To determine the α in eq. 10 we can follow several ways. If we are interested in obtaining turbulent fluxes from profiles the best way is to optimize α such that the sum of squares of the difference between the measured u_* or θ_* and the profile derived u_* or θ_* is least.

If we are interested in obtainig the universal function ϕ we should optimize the sum of squares of the differences between the measured ϕ and the calculated ϕ. In appendix A.1 it will be shown that this method suffer from bias if the basic quantities measured are finite time averages.

Also in appendix A.1 a procedure is outlined to circumvent this problem by taking 10 data points of approximately equal stability. From this 10 data-points one approximately unbiased estimate of ϕ and the related ζ are calculated together with an estimate of the standard error in ϕ. We call this method hereafter the DBEC-method (Decreased Bias Estimate through Classification).

Apart from the advantage of giving unbiased estimates this method is convenient for graphical presentation since the number of data points is considerably reduced. Since standard errors are obtained, the DBEC-method makes it possible to do a goodness of fit test of the model against the data.

Here we will primarely use the method for presenting the data in a surveyable way. All the error bars in figures presented in the next sections indicate ± 1 standard error according to the DBEC-method.

Momentum, the unstable case

The figures 4 a, b and c show the dimensionless shear for the unstable case, between the levels (a) 36 and 31 m, (b) 31 and 24 m and (c) 24 and 18 m respectively. Drawn is eq. 10 with α_M optimized for each level separately together with the curve with $\alpha_M = 1.0$. Note that the x-axis (stability) is logarithmic. Bars denote one standard error.

For the highest level the regression line fitts the data fairly well. For the lower two intervals we see a much flatter behaviour of the data as function of stability then is indicated by the regression lines. This effect is strongest at the lowest height interval. The data indicate a decreasing dimensionless shear with decreasing height.

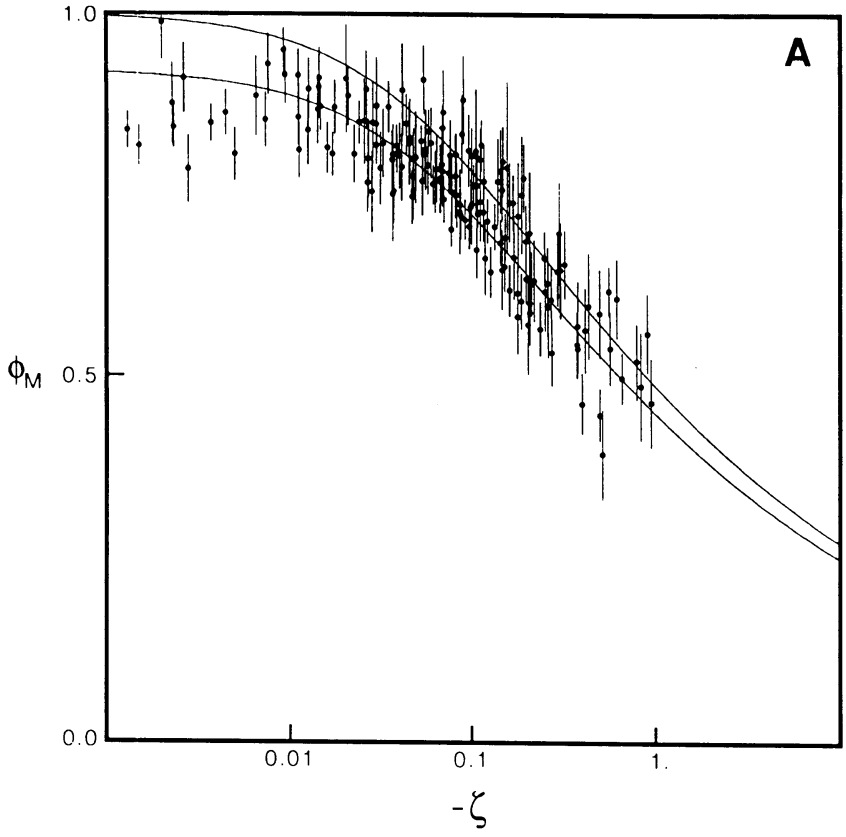
A
1.0
0.5
0.0
ϕ_M
0.01
0.1
1.
$-\zeta$

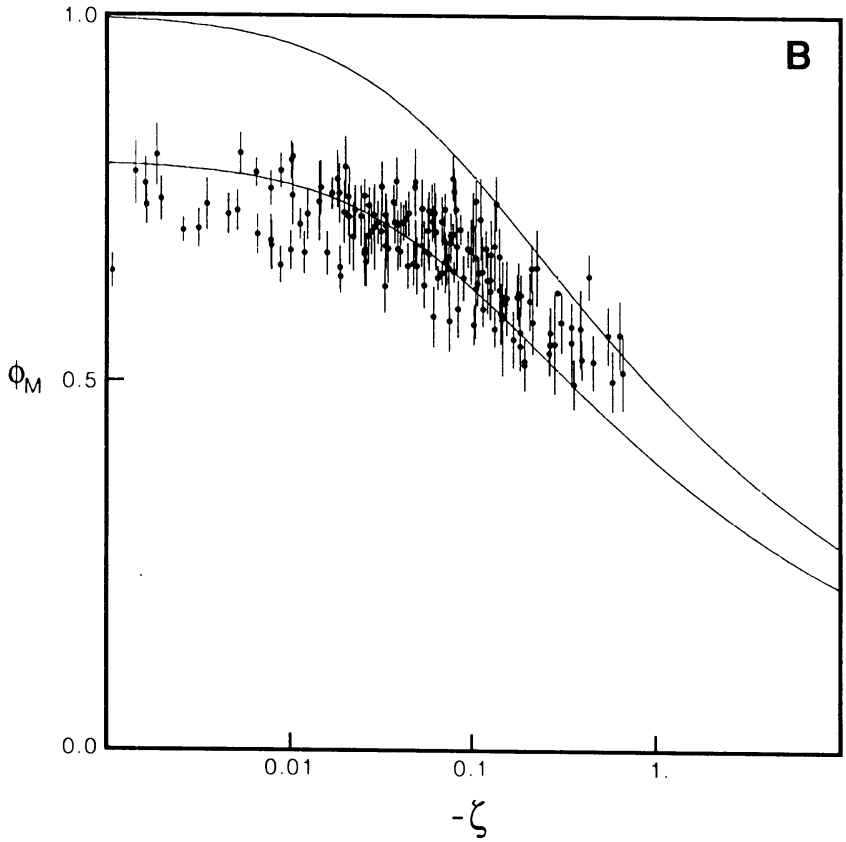
B
1.0
0.5
0.0
ϕ_M
0.01
0.1
1.
$-\zeta$

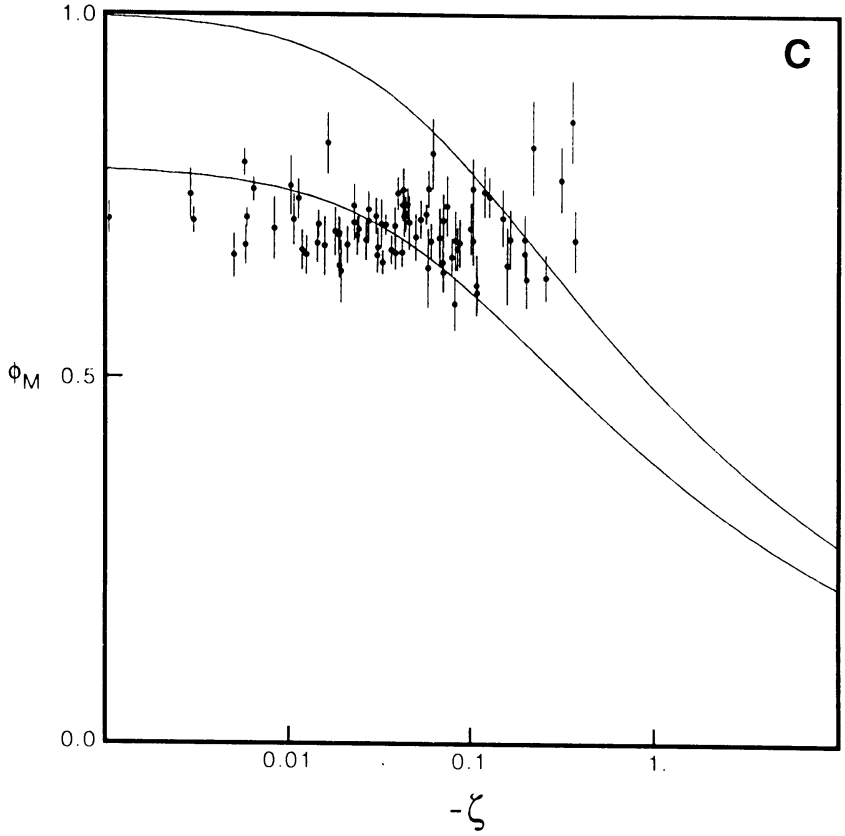

Figure 4.
Dimensionless shear for the unstable case for a) 36 - 31 m, b) 31 - 24 m, c) 24 -18 m. Drawn are the modified functions ϕ with $\alpha = 1$ and an optimized α.

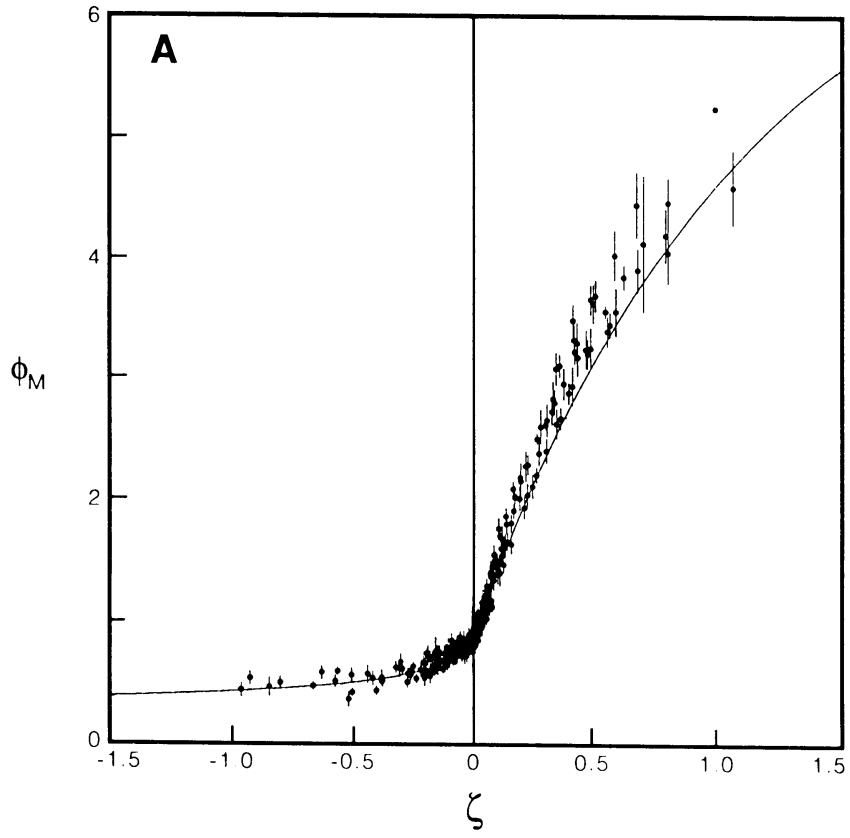

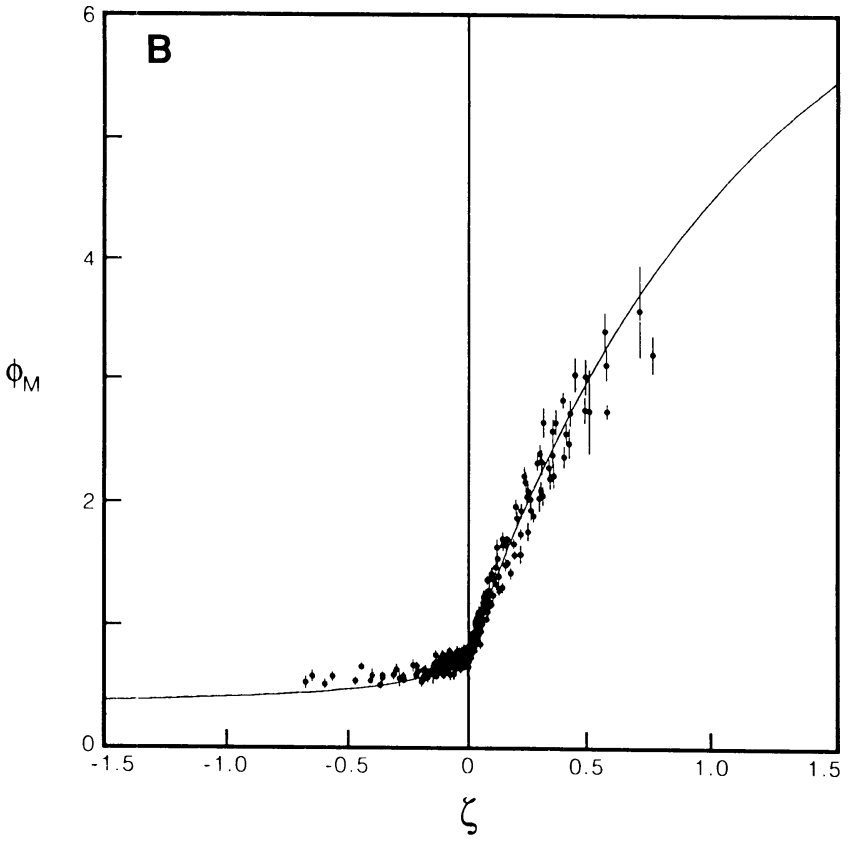

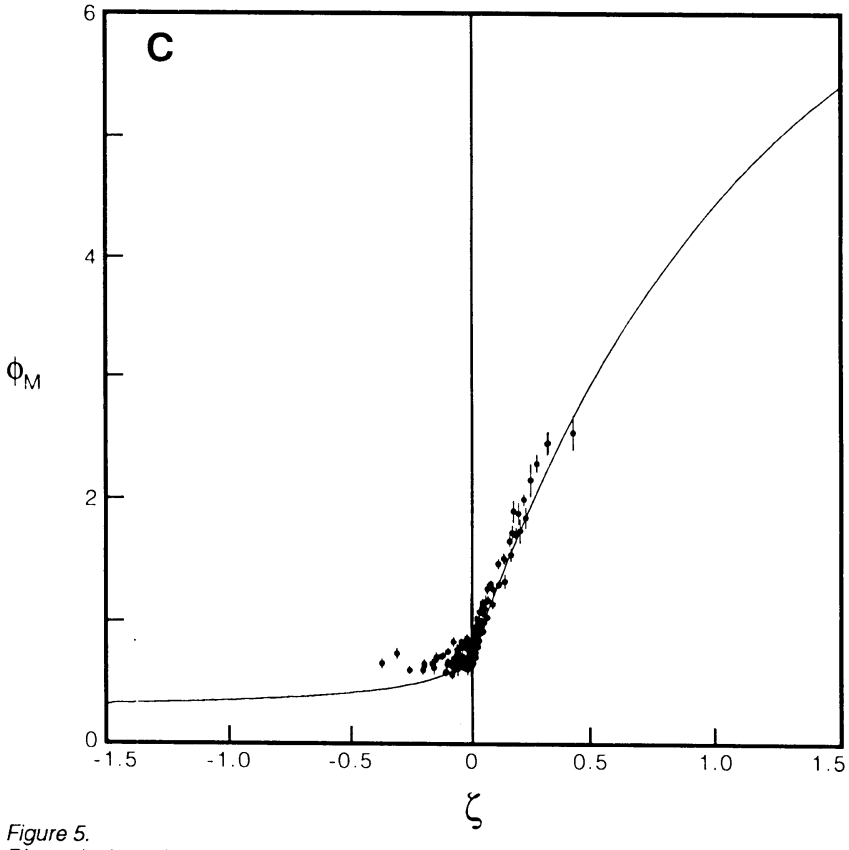

Figure 5.
Dimensionless shear for the whole stability range. a, b and c the same as in figure 4.

Momentum, the stable case

The figures 5 a, b and c show the dimensionless shear for the whole stability range. Here we concentrate on the stable side. The x-axis is linear in the stability. Drawn is the regression curve with the same α_M-value as found in figure 4.
The data follow the bending of the curve quite well. For the highest level the data tend to be lower then the curve.

Temperature, the unstable case

The figures 6 a, b and c show the dimensionless potential temperature gradient for the unstable case together with the model curve with optimized α_H and the model curve with $\alpha_H = 1.0$. In general the data follow the regression line very well for the two highest levels. The lowest level gives more scatter. Again and even more pronounced then in the momentum case the dimensionless gradients are smaller as we go down.

Temperature, the stable case

The figures 7 a, b and c show the dimensionless potential temperature gradients for the whole stability range. We concentrate on the stable side. The model curve is based on the same α_H-value as found in figure 6. Here again data follow the model curve quit well, although there is somewhat more scatter then in the momentum case. A bending trend in the measured data at higher stability is present although less pronounced then with momentum.

4.5 Height dependency

From the results presented sofar it is clear that the dimensionless gradients depend on height. This dependency can be quantified by optimizing the α-parameter in the model. In table 3 the α's are shown for temperature and momentum and for each level interval on the basis of two optimalisation strategies outlined in section 4.4:

1) half hour averaged $\phi_{\theta,M}$-values
2) half hour averaged u_*,θ_*-values.

It is seen that the two method give nearly equal result.

	$\alpha(\phi)$	$\alpha(\phi_*)$
Temperature		
36 - 31 m	0.973	0.987
31 - 24 m	0.798	0.809
24 - 18 m	0.651	0.667
Momentum		
36 - 31 m	0.968	0.968
31 - 24 m	0.841	0.833
24 - 18 m	0.858	0.844

Table 3. α-values for temperature and momentum for each height interval and for two different optimalisation methods.

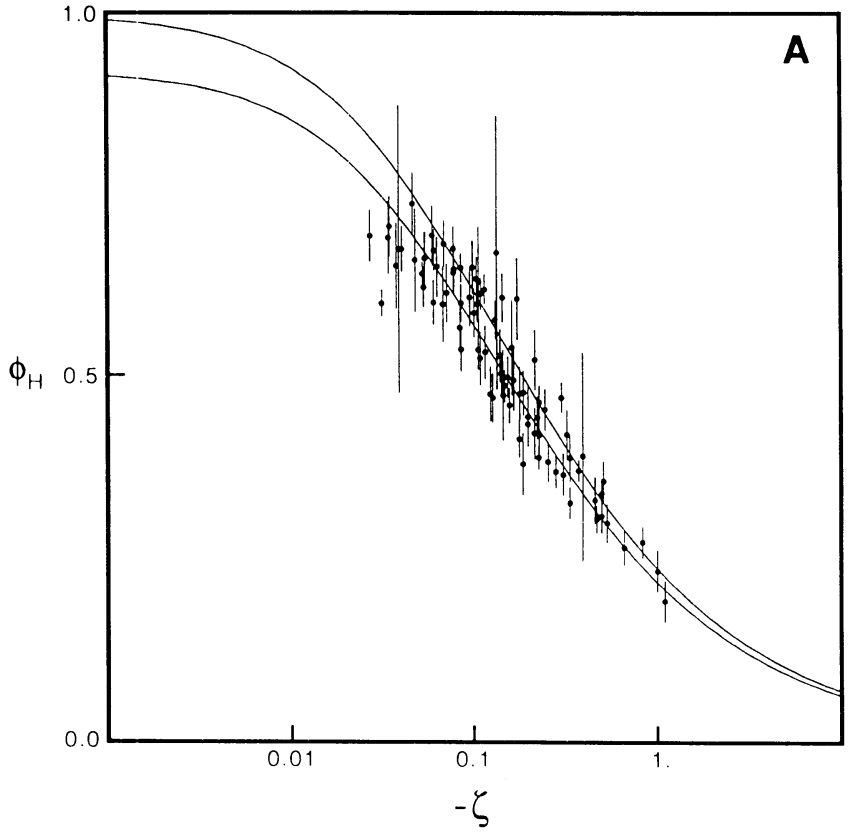
A
1.0
0.5
0.0
ϕ_H
0.01
0.1
1.
$-\zeta$

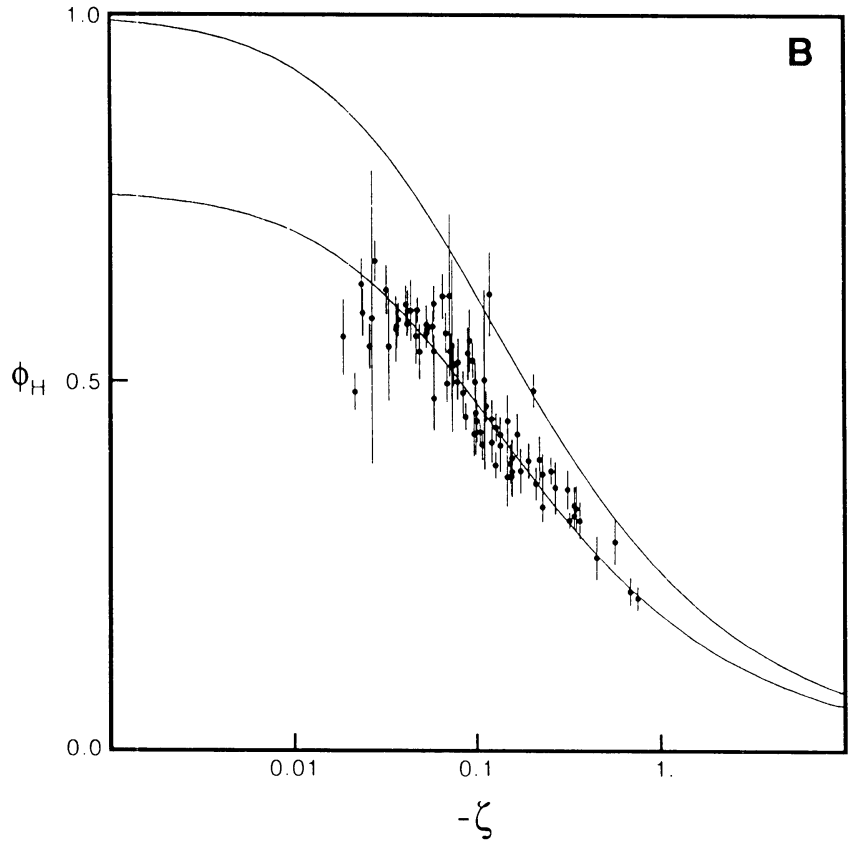
B
1.0
0.5
0.0
ϕ_H
0.01
0.1
1.
$-\zeta$

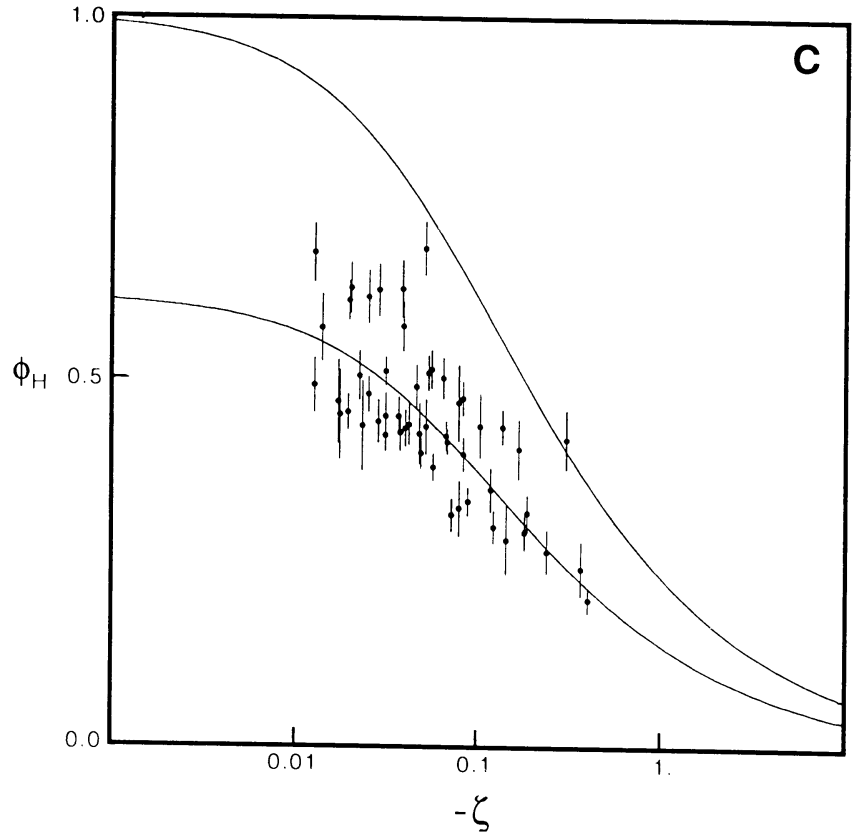

Figure 6.
Dimensionless potential temperature gradient for the unstable case. a, b and c the same as in figure 4.

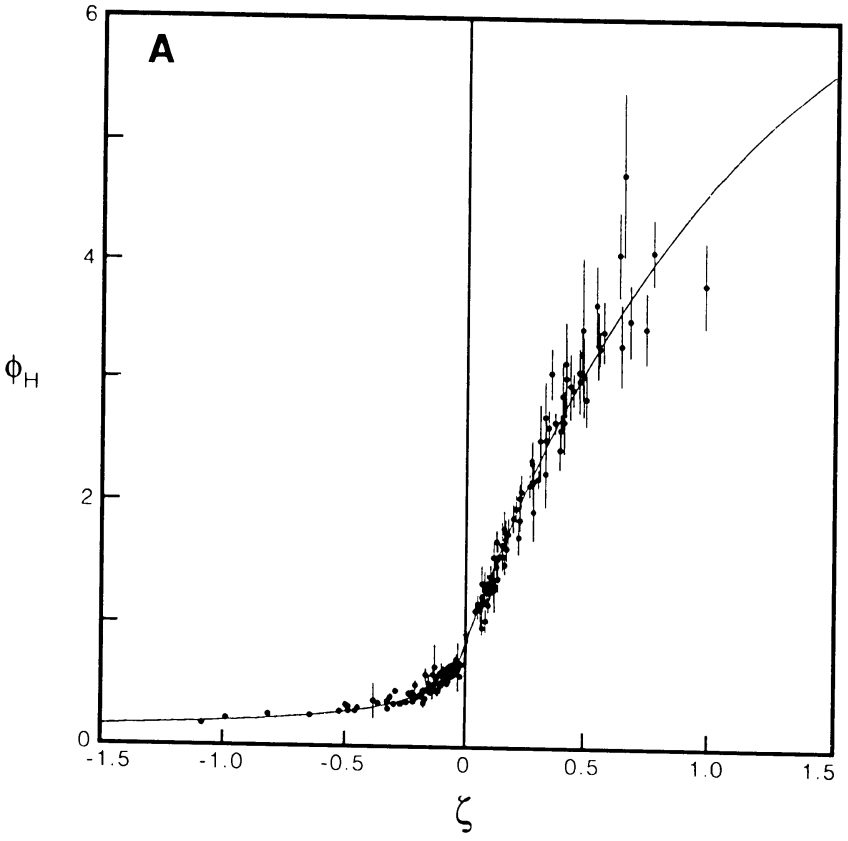

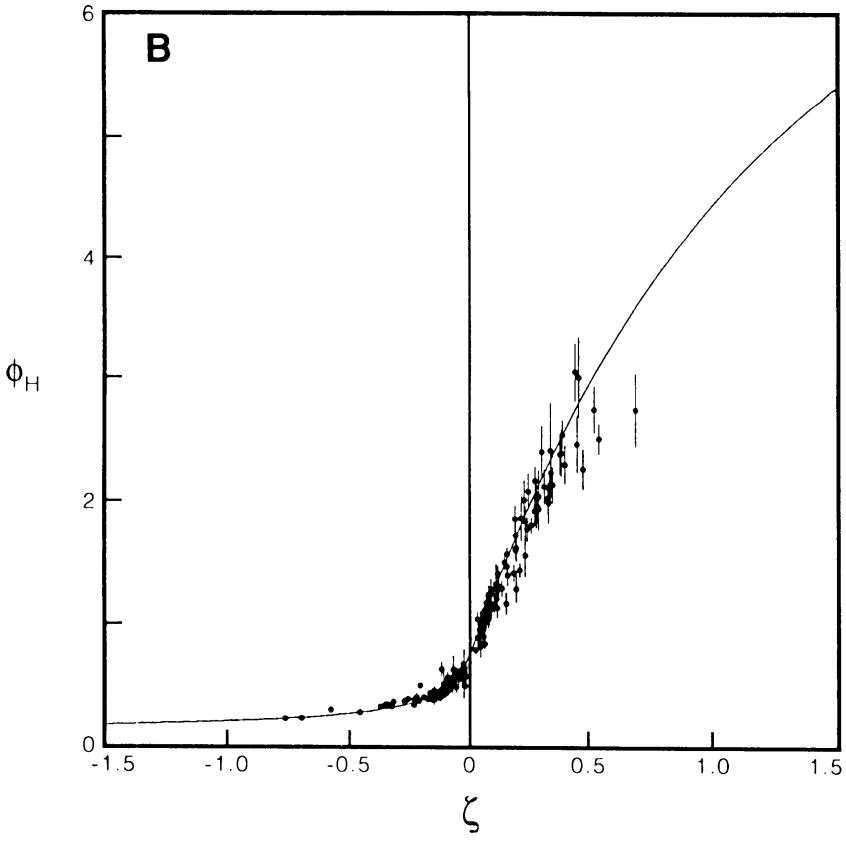

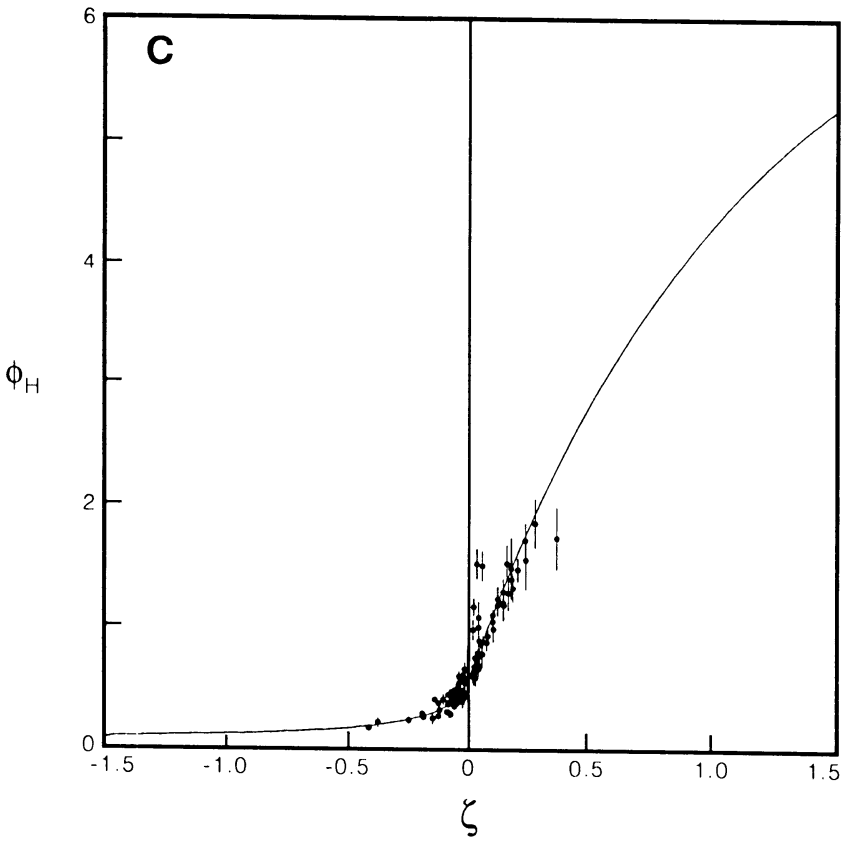

Figure 7.
Dimensionless potential temperature gradient for the whole stability range. a, b and c the same as in figure 4.

4.6 Wind direction and wind speed influence

A goodness of fit test of the model line to the data indicate that the estimated standard deviations of the individual points is to small to explain the average standard deviation of the points around the model curve. This is also true if the other parameters in the model are allowed to be optimized. This finding indicate that other factors than stability and height have influence on the dimensionless gradients too.

Wind direction dependence

The roughness length on this location is dependent on wind direction. This means that the terrain is not homogeneous with respect to momentum exchange between the atmosphere and the vegetation. So we should not be surprised to find different flux gradient relations for different wind directions. In fact there are several reasons why the flux gradient relations can depend on wind direction:

- The heather terrain in the east sector could give rise to a higher dimensionless gradient then for homogeneous terrain as discussed in section 2.
- If we interpret the average z_0 value for this location (circa 2 m) as the local value, then we have (see figure 3) rough to smooth transition in the west sector, smooth to rough transition in the south sector and no significant transition in the east sector. According to the E-ε theory the dimensionless gradients should be enhanced with southerly (low z_0) winds and reduced with westerly (high z_0) winds.
- A last factor could be a varying displacement height. On-eye inspection give some evidence for higher vegetation in the West sector and lower vegetation in the South sector relative to the local stand, while in the East sector the same height is observed.

These observations justify a classification of the data in wind direction classes, much the same as presented for the roughness length determination. A detailed analysis will be the subject of a future study. Here we try to get a more qualitative picture. Therefore we limit the analysis to the unstable case of temperature and discriminate between two winddirection classes I) 30-120° and II) 240-300°. Figure 8 a, b and c give the results for both classes. The optimized model-curves are drawn too.

It is evident that there is a significant difference between these two winddirection classes. At the highest level the ϕ-curve lays highest for the East sector. At the lowest level the ϕ-curve lays highest for the West sector. Figure 9 show the α values for the two wind direction classes together with the values for all the data as a function of effective height z_{eff} as defined in eq. 12.

Wind speed dependence

To access the influence of wind speed on the dimensionless gradients we first turn back to the estimation of the roughness length as given in section 4.3.

In practice it was found to be quit difficult to arrive at a definite z_0 value. In figure 10 kU(z)/u. is plotted against stability (L^{-1}) for the wind direction between 30 and 120°. Here each point is derived with the DBEC-method. We observe a dip in the stability curve around neutral values. The drawn line is the integrated Dyer and Hicks relation with z_0 = 1.9 m, which seems to be representative for all data except those with $|L| > 200$ m. If we use the neutral crossing value we arrive at a roughness length of 2.4 m. The values given in figure 3 are intermediar between the high and the low windspeed values.

Figure 11 shows for the wind direction 60-90° the individual half hour values. The data are

split in two windspeed classes, U_{36} > 4 m/s and U_{36} < 3.5 m/s. It is clear from the figure that the low wind speed values do not show a dip around neutral. Clearly the measurements do not follow similarity theory here for | L | > 200 m.

Figure 12 show ϕ_M for the height interval 24 - 18 m and the wind direction interval 45-90°, the individual halfhour values for | ζ | < 0.1. Again the data are split in two windspeed classes, U_{36} > 4 m/s and U_{36} < 3.5 m/s. It is observed that especially the high wind speed cases give rise to the dip in the function around neutral. Again this departure occurs for | L | > 200 m. This effect indicates a shift in turbulent structure with increasing windspeed which however seems to be absent when buyoncy effects come into play.

One could speculate about the causes. One mechanism could be the changing wake geometry relative to the tree distance as windspeed increases. A second mechanism could be the relative dominance of gusts at higher windspeeds which penetrates more easely the vegetation and therefor are more efficient for momentum exchange.

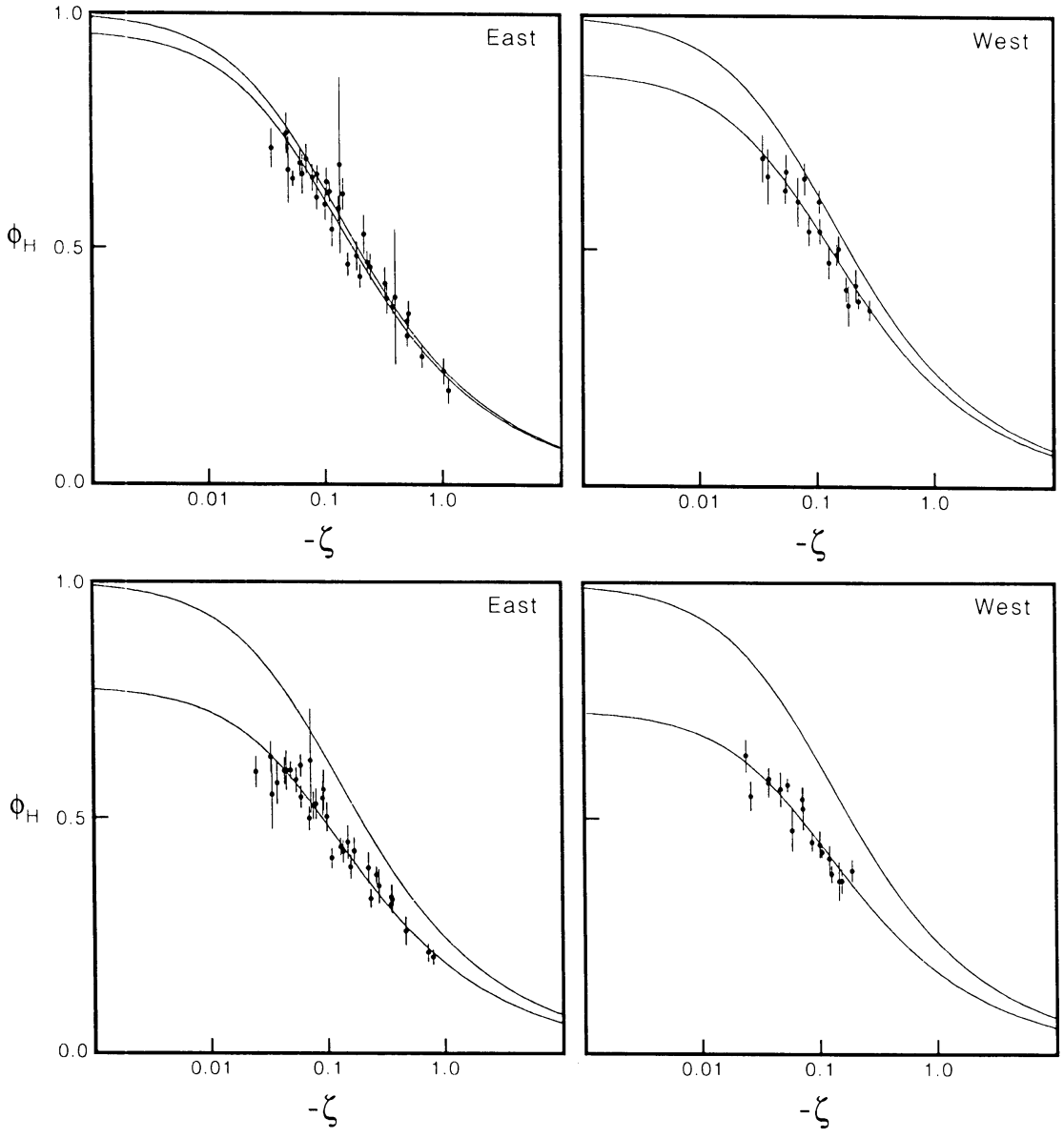

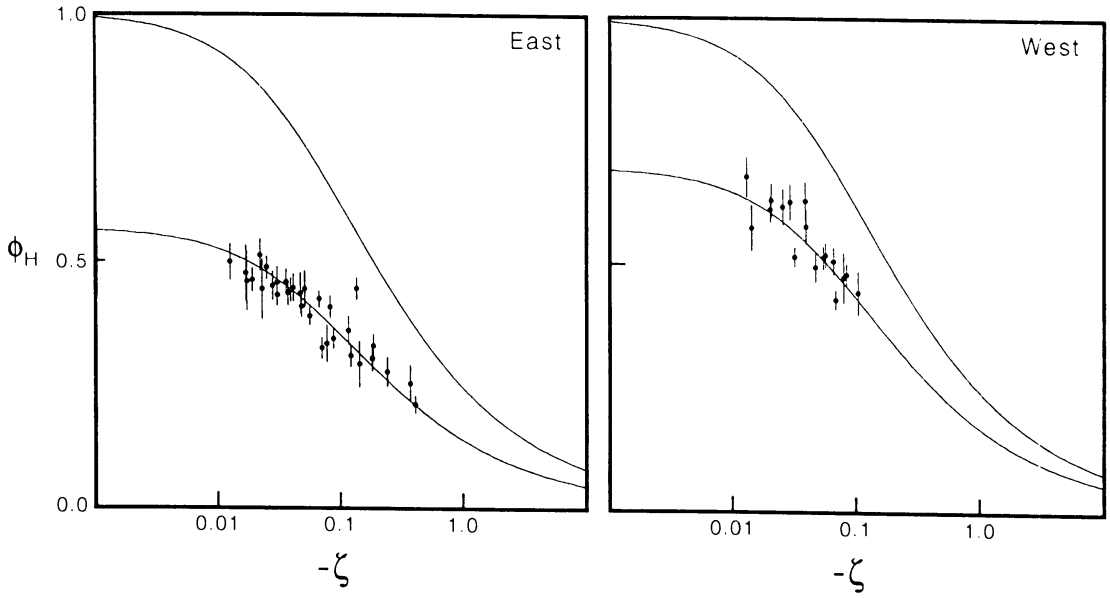

Figure 8.
Dimensionless potential temperature gradient for the unstable case, for two wond classes, East) 30-120° and West) 240-300°. a, b end c the same as figure 4.

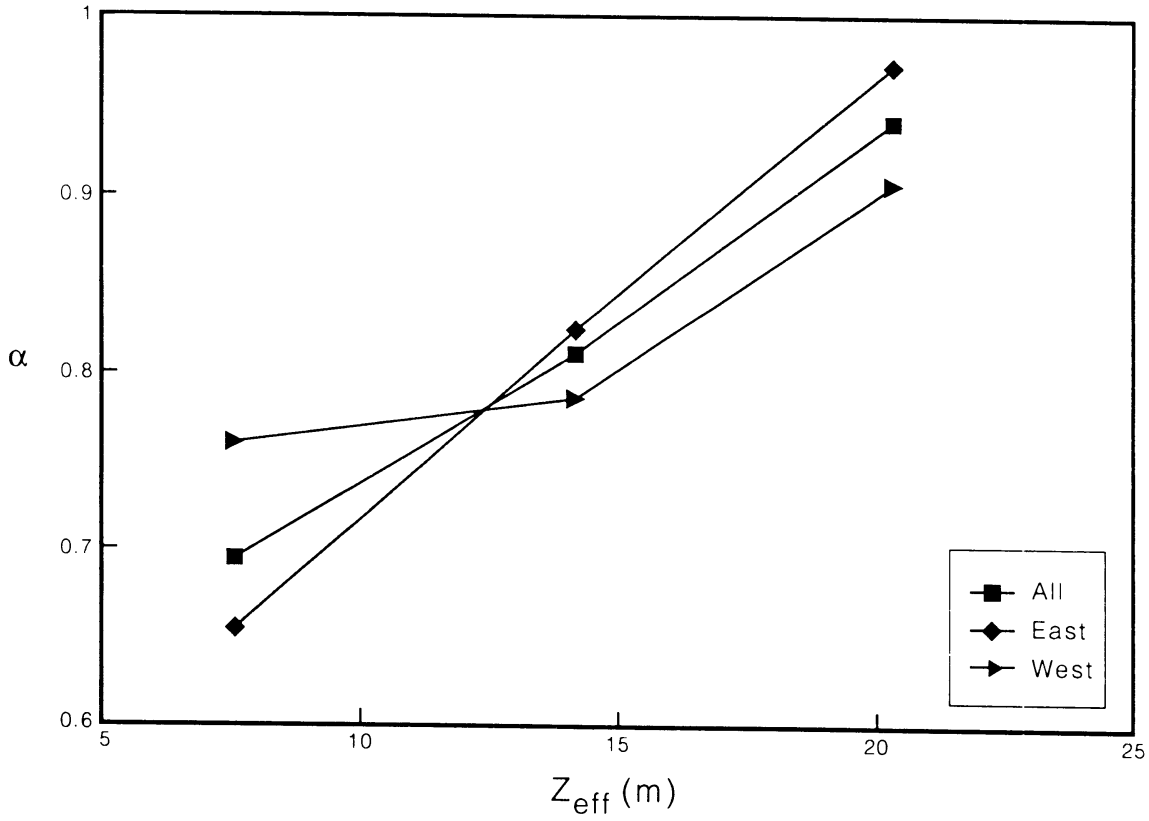

Figure 9.
α-values for temperature and for different wind directions as function of z_{eff}

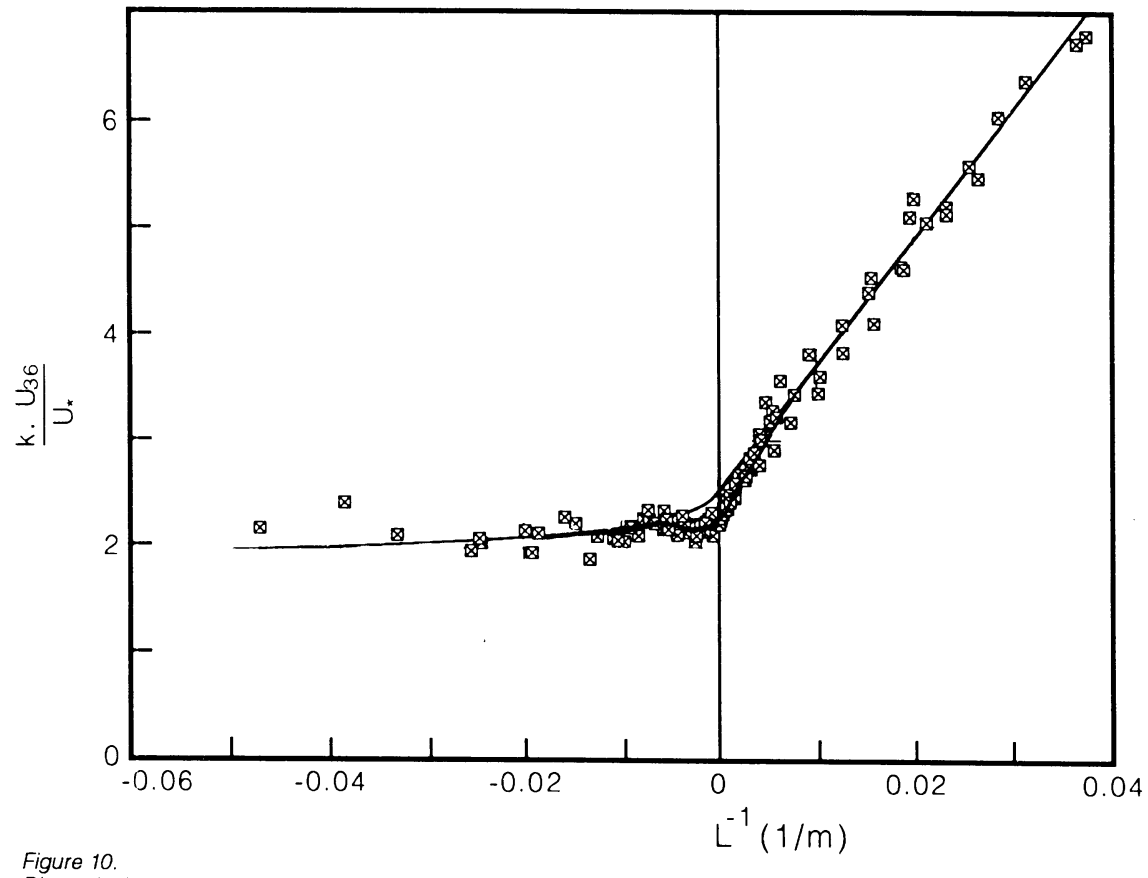

Figure 10.
Dimensionless windspeed at z = 36 m against stability (L^{-1}) for the wind direction class 30-120°.

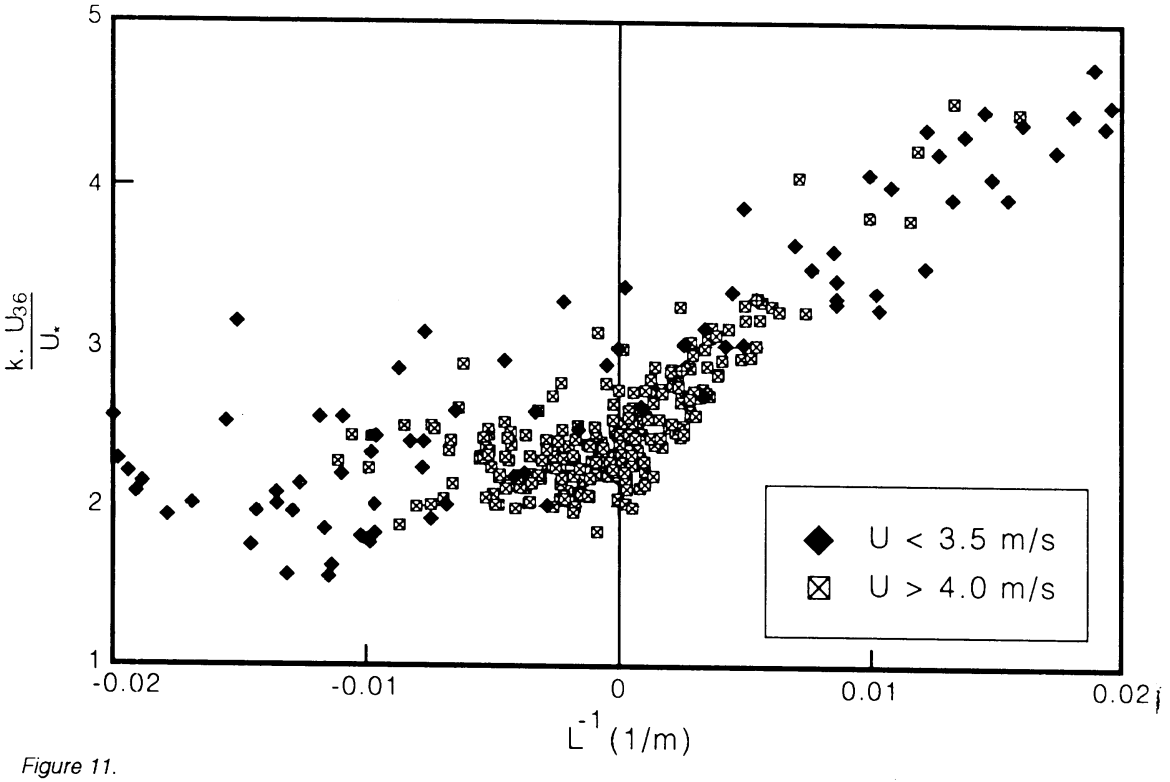

Figure 11.
Individual half hour mean values of the dimensionless wind at z = 36 m against stability (L^{-1}) for the wind direction class 60-90°. Data are split into two windspeed classes U(z=36) > 4.0 m/s and U(z=36) < 3.5 m/s.

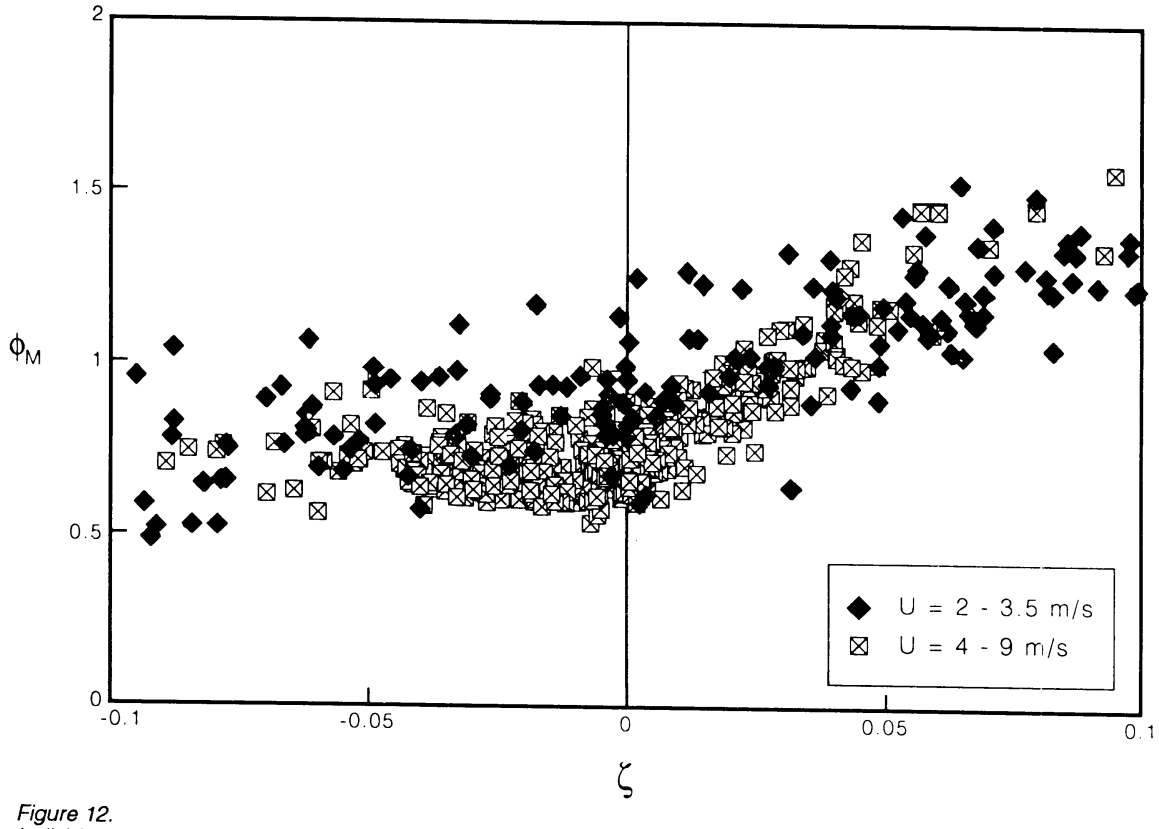

Figure 12.
Individual half hour mean values of the dimensionless wind shear between 18 and 24 m against stability (z/L) for the wind direction class 45-90°. Wind speed classes the same as in figure 11.

5. Implementation of the modified flux profile relations

From section 4.4 we can conclude that temperature gradients are well described by the modified ϕ functions when α_H is optimized for each level seperately. For momentum gradients the describtion turns out to be less good. Especially for the lower levels the dependency on stability is less pronounced as described by the modified relations or even absent. Smaller variations in the dimensionless gradients occur due to wind direction and wind speed dependency. Furthermore the discription of the stable side by the model is satisfactory.

For the purpose of deriving fluxes from vertical gradient measurements for air pollution components we take a practical approach. Firstly, we neglect the observed dependencies on windspeed and winddirection and retain the dependency on measuring height. Secondly, we are interested in obtaining u_* and θ_* values from half hour averaged gradient measurements. Thus we use the $\alpha(\theta_*)$-values given in table 2.

For the implementation we need the so-called integral forms of the dimensionless gradients. The model eq. 8 for the stable case cannot be analytically integrated. Since this description is based on the integral relations introduced by van Ulden and Holtslag (1985) we use their formulation for the stable side where necessary.

Since the modification of the dimensionless wind shear for unstable conditions is not well defined we derive u_* values from the wind speed U at the highest profile level together with the wind direction dependent roughness length as given in figure 3. Thus:

$$u_* = \frac{k \cdot U}{\ln\left(\frac{z-d}{z_0}\right) - \psi_M\left(\frac{z-d}{L}\right) + \psi_M\left(\frac{z_0}{L}\right)} \qquad (13)$$

where:
ψ_M is the integrated model relation for momentum given by:

$$y = \sqrt[4]{1 - 16 \cdot \zeta}$$

$$\zeta < 0 \qquad \psi_m(\zeta) = 2 \cdot \ln\left(\frac{1+y}{2}\right) + \ln\left(\frac{1+y^2}{2}\right) - 2 \cdot \operatorname{atan}(y) + \pi/2$$

$$\zeta > 0 \qquad \psi_m(\zeta) = -0.7 \cdot \zeta - 0.75 \cdot (\zeta - 14.2857) \cdot e^{-0.35 \cdot \zeta} - 10.71429 \qquad (14)$$

Here it is assumed that the highest profile level is above the roughness layer. The α_H-value for the highest level interval of 0.97, according to table 2, support this hypothesis.

For the estimation of the turbulent temperature scale we must integrate the relations given in eq. 10 according to:

$$\Delta\theta = \frac{\theta_*}{k} \int_{z_1-d}^{z_2-d} \frac{\alpha}{z} + \alpha \cdot \frac{\phi_H^{-1}}{z} \cdot dz \qquad L < 0$$

$$\Delta\theta = \frac{\theta_*}{k} \int_{z_1-d}^{z_2-d} \frac{\alpha}{z} + \frac{\phi_H^{-1}}{z} \cdot dz \qquad L > 0 \qquad (15)$$

To solve this relation is now somewhat complex since α is a function of height too. However, for heights not to far apart we can approximate the integral by:

$$\theta_* = \frac{k \cdot \Delta\theta_{21}}{\alpha_H \left\{ \ln\left(\frac{z_2-d}{z_1-d}\right) - \psi_H\left(\frac{z_2-d}{L}\right) + \psi_H\left(\frac{z_1-d}{L}\right) \right\}} \qquad L<0 \qquad (16)$$

$$\theta_* = \frac{k \cdot \Delta\theta_{21}}{\alpha_H \cdot \ln\left(\frac{z_2-d}{z_1-d}\right) - \psi_H\left(\frac{z_2-d}{L}\right) + \psi_H\left(\frac{z_1-d}{L}\right)} \qquad L>0 \qquad (17)$$

where:
ψ_H is the integrated model relation for temperature given by:

$$\zeta < 0 \qquad \psi_H(\zeta) = 2 \cdot \ln\left(\frac{1+\sqrt{1-16\cdot\zeta}}{2}\right)$$

$$\zeta > 0 \qquad \psi_H(\zeta) = -0.7 \cdot \zeta - 0.75 \cdot (\zeta - 14.2857) \cdot e^{-0.35 \cdot \zeta} - 10.71429 \qquad (18)$$

and α_H is chosen at the effective height z_{eff} as defined in eq. 12.

In figure 13 the α_H-values based on the θ_*-optimalisation are shown as a function of effective height. Also drawn is the linear regression through these three points given by:

$$\alpha_H(z_{eff}) = 1 - \lambda \cdot \frac{z_R - z_{eff}}{z_R} \qquad (19)$$

where λ = 0.53 and z_R = 21.2 m.

z_R is the height where α becomes 1, the expected undisturbed value. z_R can be interpreted as a measure for the roughness layer thickness.

Given an estimate of d, the displacement height and the measuring heights in the profile, eq. 16 can be used to derive the corresponding α-value for other heights and location in the stand.

It is assumed that c_s, the turbulent scale for scalar quantities, can be derived from the same equations with the corresponding concentration difference. Since stability which is based on the fluxes appear inplicit in the equations, iteration has to be applied to arrive at the fluxes. Figure 14 shows the application of this scheme for June 13th 1989 at the KNMI-tower based on the temperature difference between 36 and 24 meter.

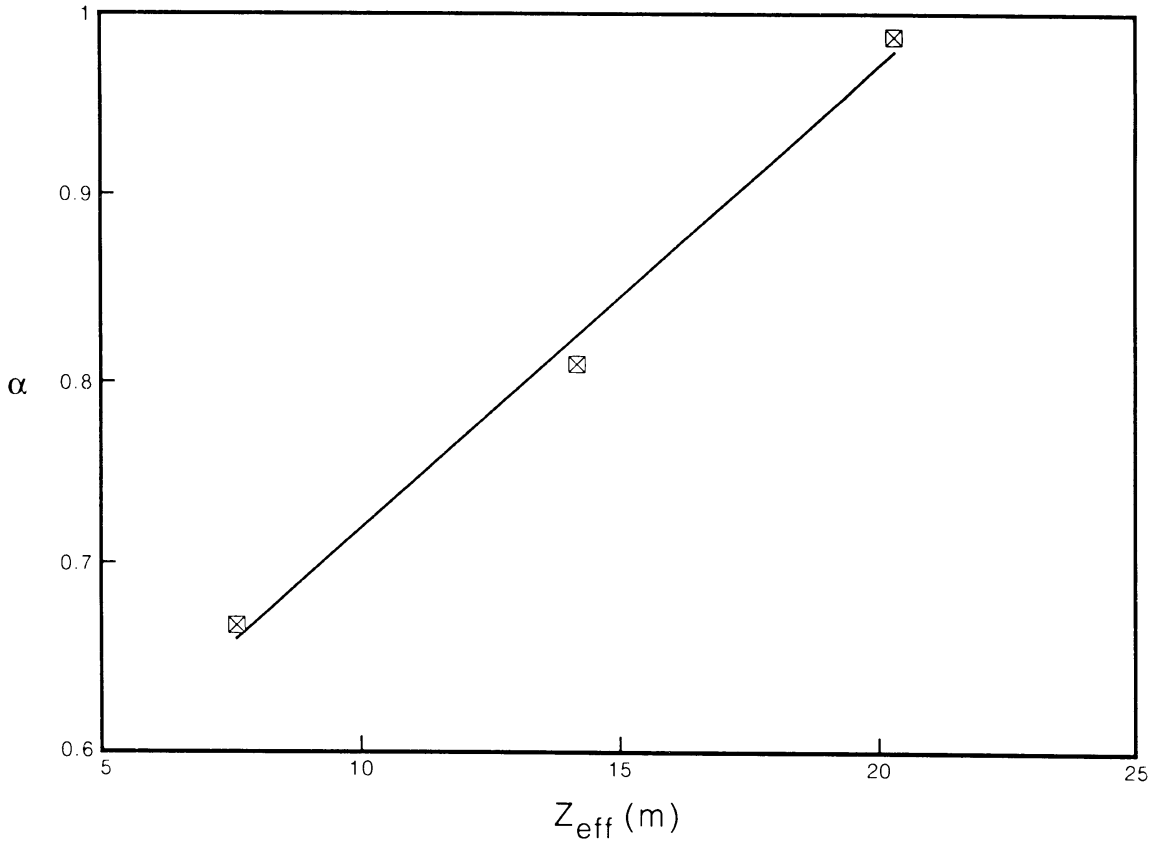

Figure 13.
Optimized α-values as a function of effective height for potential temperature.

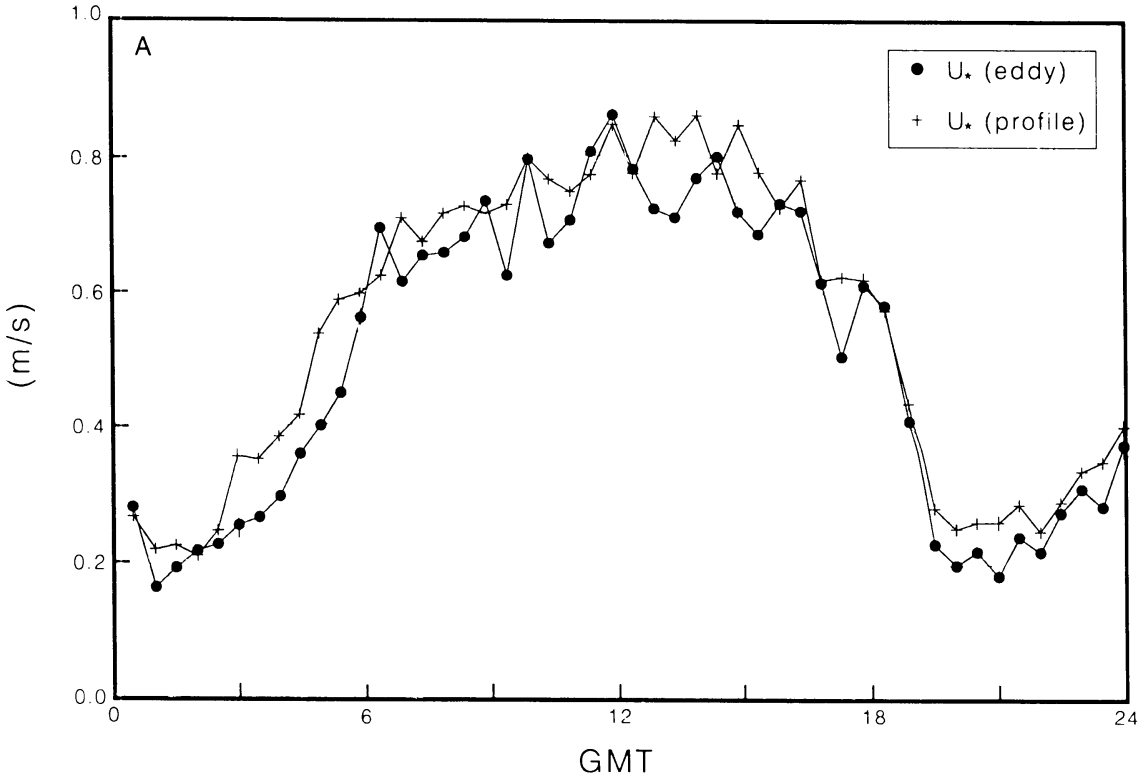

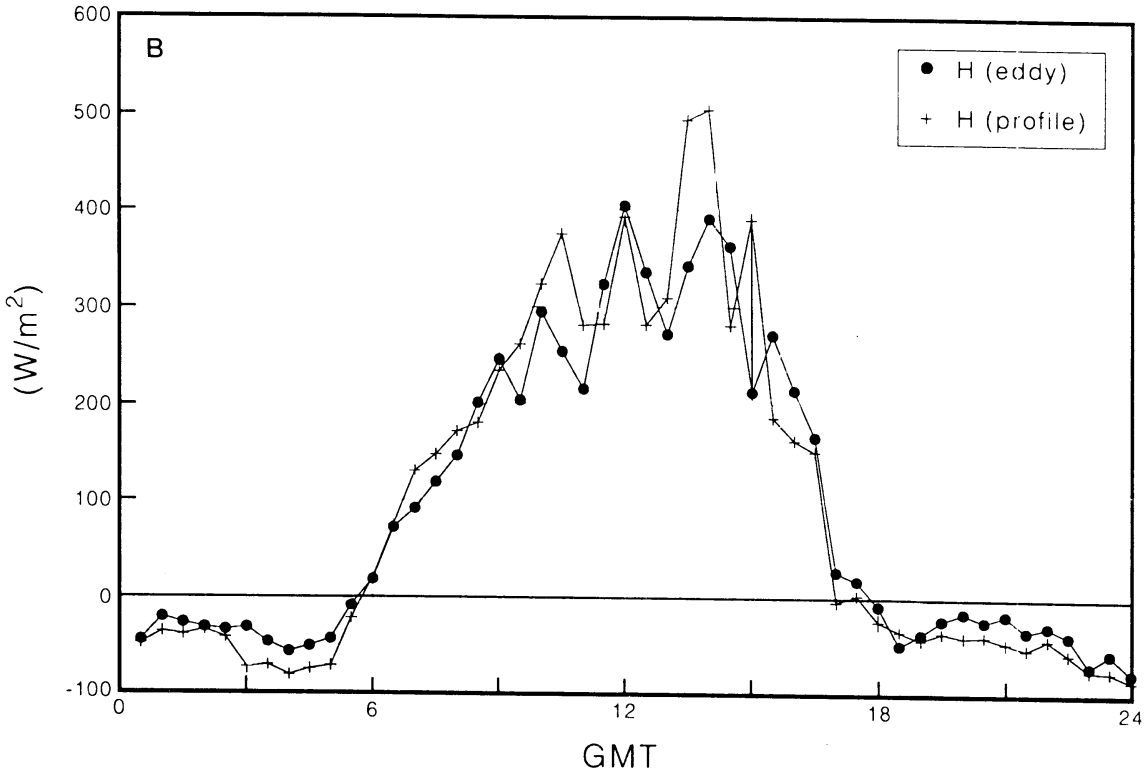

Figure 14.
Application of the flux gradient scheme to one day. a) friction velocity and b) sensible heat flux.

6. Comparison with other tower

6.1 Introduction

The 30 m high mast of the Agricultural University of Wageningen (abbriviated: LUW-mast) is located circa 120 m to the east of the KNMI-mast. On the LUW-mast profiles of wind and temperature are measured simultaneously with profiles of several air-pollution components (Vermetten,1990). Eddy-correlation measurements of wind and temperature are performed during shorter periods throughout the year on the same tower by TNO-MT.

6.2 Comparison of eddy-correlation fluxes

To determine the homogeneity of the flux-fields over the forest a comparison was made between the fluxes for momentum and temperature measured in 1989. Both quantities were measured by identical sonic anemometers at 30 m height. The sonic temperature flux <ws> was used uncorrected both for moisture and wind. The friction velocity was corrected for angle dependency and for upstream around the probe as derived by Duyzer and Bosveld (1987). No correction was made for misalignment of the probe relative to the horizontal plane or the streamlines.

Figure 15 a and b show the relation of the friction velocity and the sonic heat flux at the two locations. In both figures the data are classified according to wind direction. The wind sectors for which it is believed that no mast interference is present are indicated with black. It is seen that for these wind sectors, from 90 to 240 degrees, the deviations from the 1:1 line are smaller then for the other classes. The friction velocity show a deviation of circa 5%. For the temperature flux the deviation is circa 12%.

In view of possible error sources like non-horizontal positioning of the sonics and different obstructing geometry around the sensors which has a larger impact on momentum flux than on temperature flux measurements, we conclude that the deviations found for friction velocity is not significant from zero and the deviation of temperature flux is significantly different from zero.

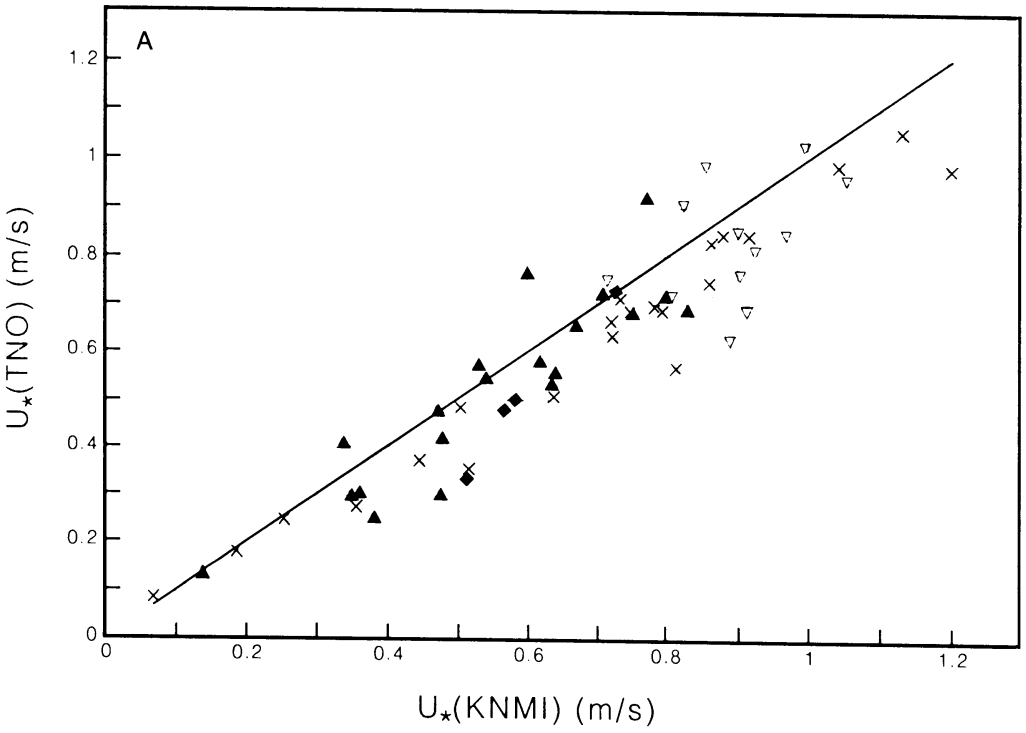

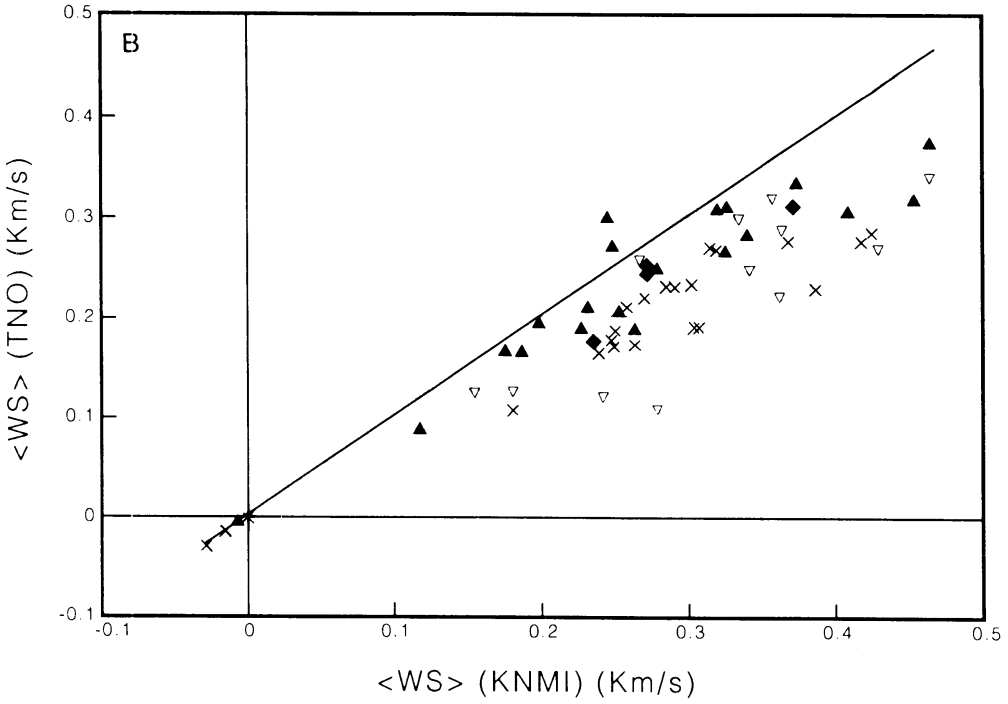

Figure 15.
Comparison of eddy-correlation fluxes measured at two masts at 120 m distance. a) friction velocity, b) temperature flux.

6.3 Comparison of profile data

The crucial point here is whether the flux-profile relations derived for the KNMI-mast can be translated to the LUW-mast. On the LUW-mast wind at 30.0 and 20.9 m, temperature at 29.6 and 20.5 m and concentrations at 29.2 and 20.1 m was measured. For this analysis one month (May 1989) of measurements were used. A first inspection of the profile measurements of temperature on the LUW-mast showed an unexpected high temperature difference between the two measuring levels, especially during low wind and high radiation conditions. The temperature sensors on the mast were not ventilated, this could be a reason for the observed deviations. It was decided to take a period with strong winds, May 20 till 24 May for further analysis.

Due to the slooping of the terrain and the somewhat lower average tree height we expected the zero-plane displacement to be 11 m near the LUW-mast instead of the 12.5 m at the KNMI-tower. This d-value was used in the analysis. When optimising θ_* for the unstable cases we arrive at $\alpha_H = 0.71$. Here θ_*-values of the KNMI-mast were used. From the translation formula eq. 16, wich is based on the KNMI-mast measurements, we derive $\alpha_H = 0.77$.

To derive fluxes from the LUW data α_H was chosen at 0.71 and d = 11 m. Figure 16 show the comparison between the profile derived u_* values at the LUW mast based on the roughness table presented in figure 3. A classification is made for stable and unstable points. The agreement for the unstable points is good, although the LUW values show less variation. This could be due to the observed wind speed dependency of roughness length wich is not accounted for in the roughness table.

For the stable points the agreement is less good especially for the low values. Aerodynamic roughness as viewed from the LUW-mast could well be somewhat different from the one observed from the KNMI-mast. However, the winddirection was mainly East during the period analysed, which is the wind direction with the most homogeneous fetch.

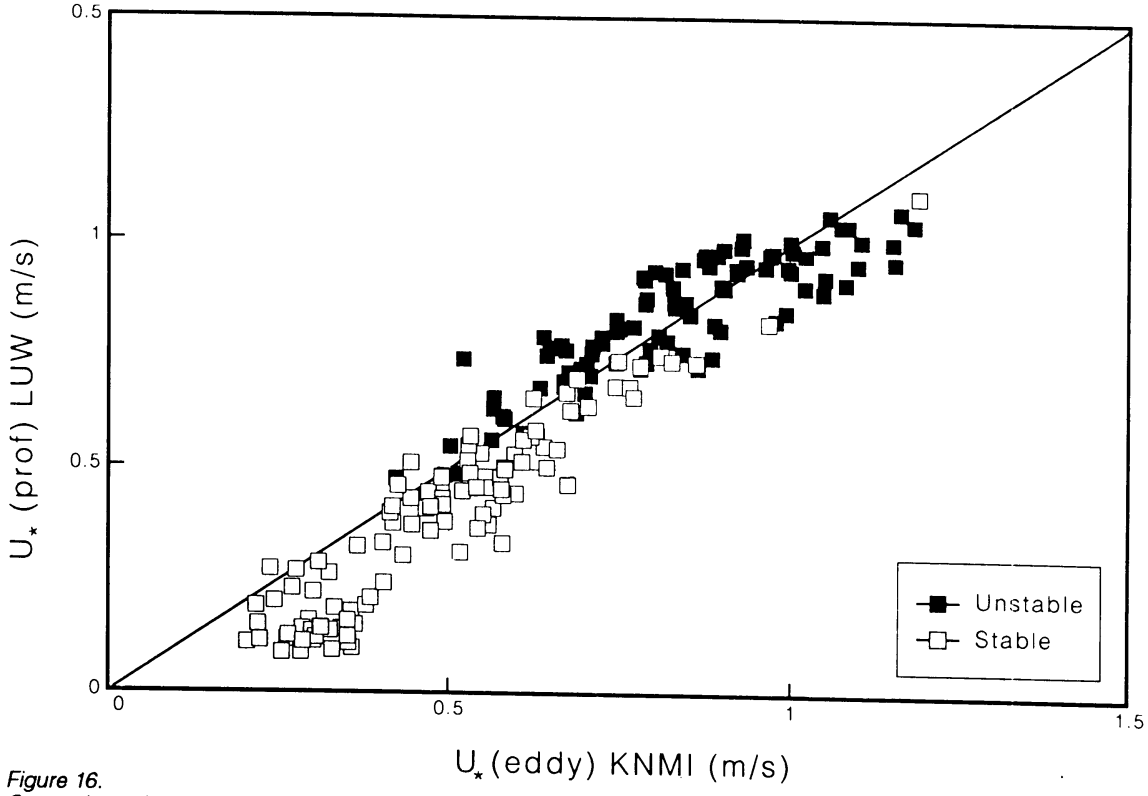

Figure 16.
Comparison of eddy-correlation friction velocities with profile derived friction velocities at two masts at 120 m distance. Classification into stable and unstable cases.

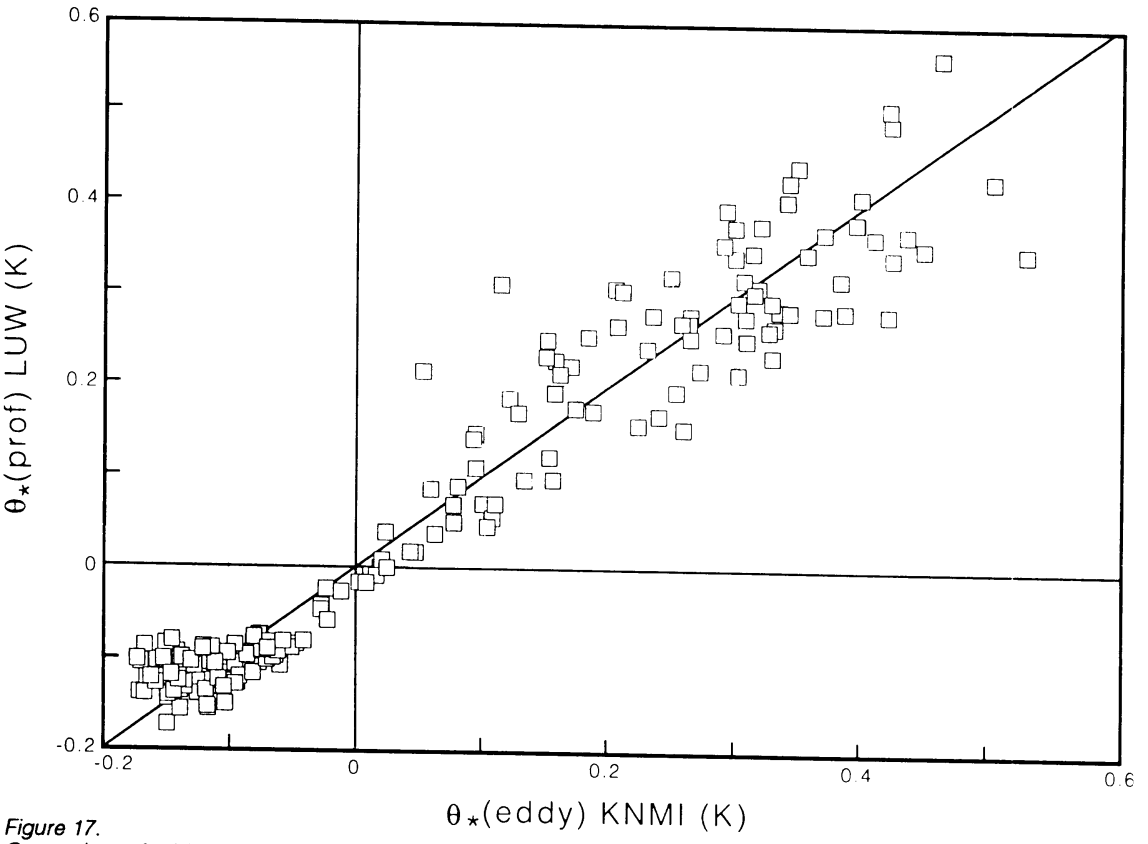

Figure 17.
Comparison of eddy-correlation turbulent temperature scale (θ_*) and profile derived θ_* at two masts at 120 m distance.

Figure 17 show a comparison between profile derived θ_*-values derived at the LUW-mast and eddy-correlation θ_*-values from the KNMI mast. Here the agreement is good for the unstable points, while for the stable points substantial relative deviations occur.

The 10% discrepancy between the α from the KNMI-mast and the α for the LUW mast can be viewed as an indication of the accuracy of the generalization of the measurements from one point above the stand to another and consequently for the interpretation of a point measurement in terms of stand average fluxes.

7. Conclusions

Well-defined flux profile relations are derived from one year of profile and turbulence measurements for momentum and temperature. It is shown that with a realistically chosen displacement height significant deviations from the usual (low vegetation) relations are found.

A strong wind direction dependence of the aerodynamical roughness length is found ranging from 1.5 to 3.0 m. This indicates substantial roughness changes near the location. The dimensionless gradients are also found to vary with wind direction and wind speed.

Modified flux-profile relations are defined which take into account the height dependence of the dimensionless gradients in the roughness layer. These modified relations give 30 to 50% higher deposition fluxes then do the low vegetation relations.

Comparison of eddy-correlation measurements from two masts at the location revealed a slight systematic difference in the heat flux. No significant difference was found for u_*-values. This indicates a relatively homogeneous heat flux and momentum flux field over the forest.

A scheme is developed for the generalisation of the modified relations to different measuring heights. This scheme is applied to translate the relations to the measuring height of a second mast. A difference of 10% was found between the translated relations and the measured relations at this second mast.

Acknowledgement

Many people have been involved during the time of this project. Without their help this project could not have been succesful. I would like to thank especially, Aart Vermetten and Jan Duyzer for delivering data and stimulating discussion, the meteorological department of the LUW for lending special cup-anemometer, M.P.D. Jansse for coordinating the technical aspects of the project, Willem Hovius, Sjaak Koster, Roel Blankenstein and Leo Schiks of the technical service of the KNMI, Mark van Wijngaarden for his assistance in designing the tower, Rob van Krimpen for tedious sensor calibrations, Gerard van der Vliet, Wim Kohsiek and Wim Monna for their assistance during the experiments, Marleen Kaltofen for typework in the final stage and the studio KNMI for drawing the figures and editing this manuscript.

A.1 Statistics with errors in independent variable

How can the universal function ϕ be derived from a data set. Imagine a field campaign during which a statistical stationary condition is persistant over the whole measuring period of say several days. With this data set we are able to derive with considerable accuracy one function-value at one stability.

What we do is determine $<\Delta U>$, the average wind difference, $<uw>$ the average stress and $<w\theta>$ the average temperature flux to derive

$$<\zeta> = -\frac{kgz}{T} \cdot \frac{<w\theta>}{<-uw>^{3/2}} \tag{A1}$$

the stability and

$$\phi_M\,(<\zeta>) = \frac{k \cdot <\Delta U>}{\Delta \ln (z)} \tag{A2}$$

What happens if we divide the time serie in blocks of length T. The averages over time T will be denoted with an index T. Then:

$$\begin{aligned} \Delta U_T &= <\Delta U> + \delta\Delta U_T \\ u_T &= <u_*> + \delta u_{*T} \\ w\theta_T &= <w\theta> + \delta w\theta_T \end{aligned} \tag{A3}$$

where the deviations result from the stochastic nature of turbulence.

We now wish to derive unbiased estimates for $<\zeta>$ and $<\phi>$ from these T-averages. The usual way is to calculate estimates for each T-period. This however results in biased estimates since ϕ and ζ are non-linear functions of the basic stochastic variables.

$$\begin{aligned} \phi_T &= \frac{k}{\Delta \ln (z)} \cdot \frac{\Delta U_T}{u_{*T}} \\ &= \frac{k}{\Delta \ln (z)} \cdot \frac{<\Delta U> + \delta\Delta U_T}{<u_*> + \delta u_{*T}} \\ &= \frac{k}{\Delta \ln (z)} \cdot <\phi> \cdot \frac{1 + \delta\Delta U_T / <\Delta U_T>}{1 + \delta u_{*T} / <u_*>} \end{aligned} \tag{A4}$$

To second order this can be written as

$$\phi_T = <\phi> \cdot \left(1 + \frac{\delta\Delta U_T}{<\Delta U>} - \frac{\delta u_{*T}}{<u_*>} + \frac{<\delta u_{*T} \cdot \delta u_{*T}>}{<u_*>^2} - \frac{<\delta\Delta U_T \cdot \delta u_{*T}>}{<\Delta U> <u_*>} \right) \tag{A5}$$

Averaging over the whole period gives:

$$\langle\phi_T\rangle = \langle\phi\rangle \cdot \left(1 + \frac{\langle \delta u_{*T} \cdot \delta u_{*T} \rangle}{\langle u_* \rangle^2} - \frac{\langle \delta \Delta U_T \cdot \delta u_{*T} \rangle}{\langle \Delta U \rangle \langle u_* \rangle} \right) \tag{A6}$$

The second term in brackets represents the variance of a friction velocity estimate on the basis of a T-period.

From Wyngaard (1973) we estimate for T = 1800 s and z = 20 m this term to range from circa 2% for neutral conditions to probably 4% for unstable cases. The third term is likely to be negative since a high u_* is likely to generate a smaller ΔU.
A similar analysis for ζ yield:

$$\langle\zeta_T\rangle = \langle\zeta\rangle \cdot \left(1 + 6 \frac{\langle \delta u_{*T} \cdot \delta u_{*T} \rangle}{\langle u_* \rangle^2} - 3 \frac{\langle \delta w\theta_T \cdot \delta u_{*T} \rangle}{\langle w\theta \rangle \langle u_* \rangle} \right) \tag{A7}$$

Since $w\theta$ and u_* are driven by quit independent processes, net-radiation and windspeed respectively, it is unlikely that the 3rd term is very high.

Assume the second term on the r.h.s of eq. 6 to be 0.03 and the third -0.015 then we have $\langle\phi_T\rangle = 1.045 \langle\phi\rangle$ and $\langle\zeta_T\rangle = 1.18 \langle\zeta\rangle$. If we adopt the Dyer and Hicks relation for momentum; $\langle\phi\rangle = (1\text{-}16\langle\zeta\rangle)^{1/4}$ then we find:

$$\langle\phi_T\rangle = \frac{1.045}{\left(1 - 13.5 \langle\zeta_T\rangle\right)^{1/4}} \tag{A8}$$

which is a clear overestimation of the true universal function.

As stated before the problem arise from the necessity to evaluate a non-linear combination of stochastic variables. If we new the statistical distribution of all the relevant combinations of variables we could correct for the bias. However in practice such knowledge is lacking and we have to turn to other methods.

A different approach is what we call Decreased Bias Estimate through Classification (DBEC). Given the T-period average values we classify the data according to the T-period stability estimates. In each class the basic T-period quantities are simply averaged and afterwards the estimates of the universal functions are made. Since the bias is kwadratic in the fluctuations this procedure diminishes the bias proportional to the number of T-periods in that class. There is now another problem which is probably mainly of a theoretical character. The statistics of this VRC-estimate is very difficult to assess, since in an ensemble of equivalent runs the partitioning of the different T-periods over the classes changes.

On the other hand the advantage of classification is that a standard error can be calculated for each class without the nessessity to know the errors in the individual T-period values. Here we calculate the standard error for each class as the standard deviation of the T-period ϕ estimates within one class. This is probably a slight overestimation.

A further refinement is obtained by weighing the T-periods within one class with the square

root of the wind speed. This account for the better statistics of high windspeed T-period measurements due to the advection of more eddies along the sensor.

Table 4 lists, analoguous to table 3 in section 4.5, the α-values for individual halfhour ϕ-values and estimates of ϕ on the basis of the DBEC-method. It is seen that the DBEC-method give 4 to 6% lower values then direct optimalisation on halfhour ϕ-values. This is in reasonable agreement with the previous estimation of the bias.

	α(DBEC)	$\alpha(\phi)$
Temperature		
36 - 31 m	0.924	0.973
31 - 24 m	0.761	0.798
24 - 18 m	0.616	0.651
Momentum		
36 - 31 m	0.924	0.968
31 - 24 m	0.802	0.841
24 - 18 m	0.790	0.858

Table 4. α-values for temperature and momentum for each height interval and for two different optimalisation methods.

A.2 Sensitivity to the choice of displacement height

Since we have prescribed the displacement height rather arbitrary in chapter 4, we analyse the sensitivity of α for different d-values. Dimensionless gradients are derived from

$$\frac{k}{\theta_*} \cdot \frac{\Delta\theta}{\Delta \ln (z\text{-}d)} = \alpha_H (d) \cdot \phi_H \qquad \text{(A9)}$$

The dependency of a on d is then given by:

$$\alpha (d) = \alpha (d_0) \cdot \frac{\ln\left(\frac{z_2\text{-}d_0}{z_1\text{-}d_0}\right)}{\ln\left(\frac{z_2\text{-}d}{z_1\text{-}d}\right)} \qquad \text{(A10)}$$

Figure 18 show the α-values for the three different height intervals as function of the prescribed d-value. To get all α's approximately equal we have to choose unrealistic low values for d, between 3 and 7 m. Moreover the α-values are then significantly larger then 1, which can not be explained by roughness layer effects.

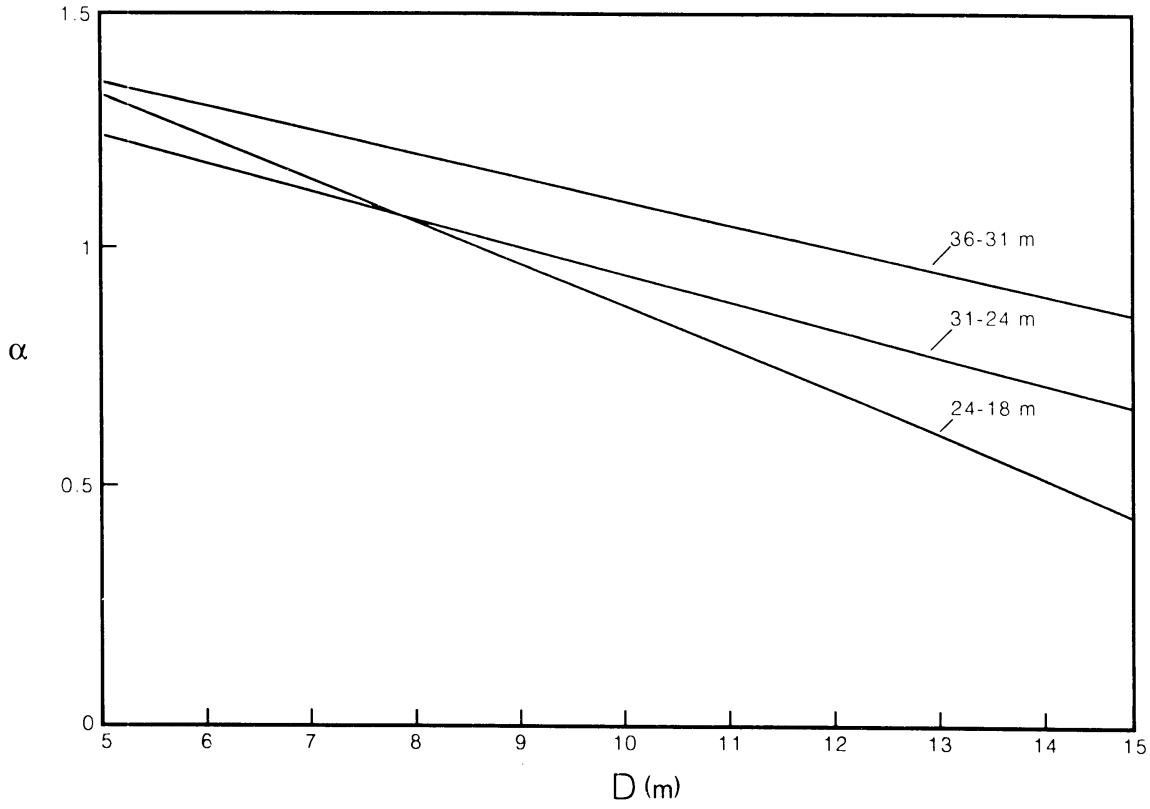

Figure 18.
Dependency of estimated α-values on assumed displacement height (D).

Literature

Arya S.P., 1991.
Finite-difference errors in estimating of gradients in the atmospheric surface layer. Journal of Applied Meteorology, 30, pp 251-253.

Beljaars A.C.M., J.L. Walmsley and P.A.Taylor, 1987.
Modeling of Turbulence over low hills and varying surface roughness. Boundary Layer Meteorology, 41, pp 203-215.

Bosveld F.C. and A.C.M. Beljaars, 1988.
Complex terrain effects on dry deposition, in: Air pollution modelling and its application VI, H. van Dop (ed), NATO challenges of modern society, Vol 11, pp 87-98, New York.

Businger J.A., 1986.
Evaluation of the accuracy with which dry deposition can be measured with current micro meteorological techniques. Journal of Climate and Applied Meteorology, 25, pp 1100-1124.

Carson D.J. and P.J.R. Richards, 1987.
Modelling surface turbulent fluxes in stable conditions. Boundary Layer Meteorology, 14, pp 67-81.

Denmead O.T.and E.F. Bradly, 1985.
Flux gradient relationships in a forest canopy, in B.A.Hutchison and B.B.Hicks (eds), The Forest-Atmosphere Interaction. Dordrecht, Riedel.

Duyzer J.H. and F.C. Bosveld, 1988.
Measurements of dry deposition fluxes of O3, NOx, SO2 and particles over grass/heathland vegetation and the influence of surface inhomogeneity, Dutch priority program on acidification Report no 99-3. TNO-MT Report no R 88/111. Delft, TNO.

Dyer A.J., 1974.
A review of flux-profile relationships. Boundary Layer Meteorology, 7, pp 363-372.

Fazu C. and P. Schwerdtfeger, 1989.
Flux-gradient relationships for momentum and heat over a rough natural surface. Quart.J.Royal Met.Soc., 115, pp 335-352.

Garratt J.R., 1978.
Flux profile relations above tall vegetation, Quart.J.Royal Met.Soc., 104, pp 199-221.

Hicks B.B., 1976.
Wind profile relationships from the Waranga experiment. Quart. J. Roy. Met. Soc., 102, pp535-551.

Högström U., H. Bergström, A. Smedman and S. Halldin, 1989.
Turbulent exchange above a pine forest, 1: fluxes and gradients. Boundary Layer Meteorology, 49, pp 197-217.

Holtslag A.A.M. and A.P. van Ulden, 1983.
A simple scheme for daytime estimates of the surface fluxes from routine weather data. Journal of Climate and Applied Meteorology, 22, pp 517-529.

Jackson P.S., 1981.
On the displacement height in the logarithmic velocity profile. Journal of Fluid Mechanics, 111, pp 15-25.

Raupach M.R., 1979.
Anomalies in flux-gradient relationships over forest. Boundary Layer Meteorology, 16, pp 467-486.

Schotanus P., F.T.M. Nieuwstadt, H.A.R. de Bruin, 1983.
Temperature measurements with a sonic anemometer and its application to heat and moisture fluxes, Boundary Layer Meteorology, 26, pp 81-93.

Slob W.H., 1978.
The accuracy of aspiration thermometers, KNMI scientific report WR 78-1. De Bilt, KNMI.

Thom A.S., 1971.
Momentum absorption by vegetation, Quart. J. Royal Met.Soc., 97, pp 414-428.

Van Ulden A.P. and A.A.M. Holtslag, 1985.
Estimation of atmospheric boundary layer parameters for diffusion application. J. of Climate and Applied Meteorology, 24, pp 1196-1207.

Vermetten A., P.Hofschreuder and A.H.Versluis, 1990.
Air pollution in forest canopies. Dutch Priority Program on Acidification, Project nr 101-09. Wageningen, Agricul. Univ. rep. R-424

Wyngaard J.C., 1973.
On surface layer turbulence. In: D.A.Haugen (ed), Workshop on Micrometeorology. Boston, Am. Met. Soc.